https://doi.org/10.1016/j.ejmech.2019.04.008

Design, Synthesis and Biological Evaluation of Pyridine-Chalcone Derivatives as Novel Microtubule-Destabilizing Agents

Feijie Xu[a,#], Wenlong Li[a,#], Wen Shuai[a], Limei Yang[a], Yi Bi[b], Cong Ma[c], Hequan Yao[a], Shengtao Xu[a,*], Zheying Zhu[d], Jinyi Xu[a,*]

[a]State Key Laboratory of Natural Medicines and Department of Medicinal Chemistry, China Pharmaceutical University, 24 Tong Jia Xiang, Nanjing 210009, P. R. China

[b]School of Pharmacy, Key Laboratory of Molecular Pharmacology and Drug Evaluation, Yantai University, Yantai 264005. P. R. China

[c]State Key Laboratory of Chemical Biology and Drug Discovery, and Department of Applied Biology and Chemical Technology, The Hong Kong Polytechnic University, Kowloon, Hong Kong

[d]Division of Molecular Therapeutics & Formulation, School of Pharmacy, The University of Nottingham, University Park Campus, Nottingham NG7 2RD, U. K.

 # These authors contributed equally to this work.

***Corresponding Author:**
E-mail addresses: cpuxst@163.com (S. Xu); jinyixu@china.com (J. Xu)

Abstract

Further optimization of the trimethoxyphenyl scaffold of parent chalcone compound (**2a**) by introducing a pyridine ring afforded a series of novel pyridine-chalcone derivatives as potential anti-tubulin agents. All the target compounds were evaluated for their antiproliferative activities. Among them, representative compound **16f** exhibited the most potent activity with the IC_{50} values ranging from 0.023 to 0.045 μM against a panel of cancer cell lines. Further mechanism study results demonstrated that compound **16f** effectively inhibited the microtubule polymerization by binding to the colchicine site of tubulin. Moreover,

cellular mechanism studies disclosed that **16f** caused G2/M phase arrest, induced cell apoptosis and disrupted the intracellular microtubule network. Also, **16f** reduced the cell migration and disrupted the capillary-like tube formation of human umbilical vein endothelial cells (HUVECs). Importantly, **16f** significantly inhibited tumor growth in H22 xenograft models without apparent toxicity, which was stronger than the reference compound CA-4, indicating that it is worthy to investigate **16f** as a potent microtubule-destabilizing agent for cancer therapy.

Keywords: pyridine; chalcone; microtubule-destabilizing agent; colchicine site; anti-vascular; antitumor

1. Introduction

Microtubules as the key components of the cytoskeleton, are long, filamentous, tube-shaped protein polymers which are essential in all eukaryotic cells [1]. Microtubules, which are composed of α-tubulin and β-tubulin heterodimers, play vital roles in cell proliferation, trafficking, signaling, migration, cell division and mitosis [2]. For this reason, microtubules become an important target for anticancer drugs. Microtubule-active drugs generally bind to one of three main classes of sites on tubulin, the paclitaxel site, the vinca domain and the colchicine domain [3]. Those inhibitors that bind to the taxane or vinca alkaloid binding sites have many disadvantages such as extremely structural complexity, low aqueous solubility, multidrug resistance and dose-limiting toxicity [4]. Hence, colchicine binding site inhibitors (CBSIs) are undergoing intensive investigation in recent decades [5].

Combretastatin A-4 (**1**, CA-4), an excellent colchicine binding site inhibitor which was isolated from the bark of the African willow tree *Combretum caffrum*, displayed potent antimitotic and vascular disrupting profiles [6]. Other typical colchicine binding site inhibitors were chalcone compounds **2a** and **2b** which were discovered by Ducki *et al*. in 1998, both showing remarkable antiproliferative activities [7]. The 3,4,5-trimethoxyphenyl (TMP) moiety of CA-4 was vital for its activity since the 4-methoyl group formed a critical hydrogen bond with the residue Cys241 [8-10].

Attempts to modify the TMP moiety usually led to reduced anticancer potency [11-14]. However, in 2017, Yin *et al.* introduced a selenium atom to replace the oxygen atom at the C-3 position of TMP to afford compound **3a**, which showed improved activities both *in vitro* and *in vivo* compared to its parent compound isocombretastatin A-4 (IsoCA-4) [15]. Recently, Li *et al.* discovered a unique 3-methoxybenzo[4,5]-dioxene moiety **3b** which exhibited improved antiproliferative activity compared with the compound bearing TMP moiety [16]. Other efforts have also been made to discover new moieties to replace the TMP moiety. In 2015, Alami and colleagues reported the discovery of compound **3c** which bears a quinazoline nucleus [17], and it displayed nanomolar-level cytotoxicity against various human cancer cell. In 2017, Alami's group reported an isoCA-4 analog **3d** with a quinoline moiety [18]. In 2018, Millier *et al.* first reported the high-resolution X-ray crystal structure of the heterocyclic-fused pyrimidine compound **3e** complexed with tubulin, and the results showed that the *N*-1 atom formed hydrogen bond with the residue Cys241, demonstrating that quinoline or quinazoline moieties that have *N*-1 atom might be the suitable surrogates of the traditional TMP moiety for binding to the colchicine site [19]. Meanwhile, our group also discovered a quinoline-chalcone compound **3f** by replacing TMP with quinoline moiety, and its antiproliferative activity was improved for 8-10 folds as well as the improvement of the solubility [20].

Nitrogenous heterocycles, such as pyridine, quinoline, pyrimidine and piperidine, are privileged building blocks in drugs [21]. Pyridine plays important roles in drug development, which can be found in a vast number of drugs like imatinib [22], telithromycin [23], indinavir [24] and acalabrutinib [25]. Even though the number of CA-4 analogs has been more than 28000 [26], compounds containing pyridine ring replacing of TMP have rarely been reported.

Recently, our group has focused on discovering and developing novel anticancer agents targeting tubulin-microtubule system, such as chalcone analogs bearing vinyl sulfone skeleton [27], 4-arylisochromenes [28], quinazolines that occupy three zones of colchicine domain [29] and quinoline-indole derivatives [30]. Inspired by Millier's work [19], we assumed that the *N*-1 atom of pyridine might also form a hydrogen

bond with Cys241 in the colchicine, thus pyridine might be introduced into the structures of CBSIs as an alternative ring of TMP moiety.

In this work, we continued our efforts in the modification works of the parent compound **2a** by replacing the TMP moiety with a pyridine ring. Thus, a series of novel pyridine-chalcone derivatives were designed and synthesized (Figure 2). Herein, we would like to report the synthesis and evaluation of their antitumor activities *in vitro* and *in vivo*.

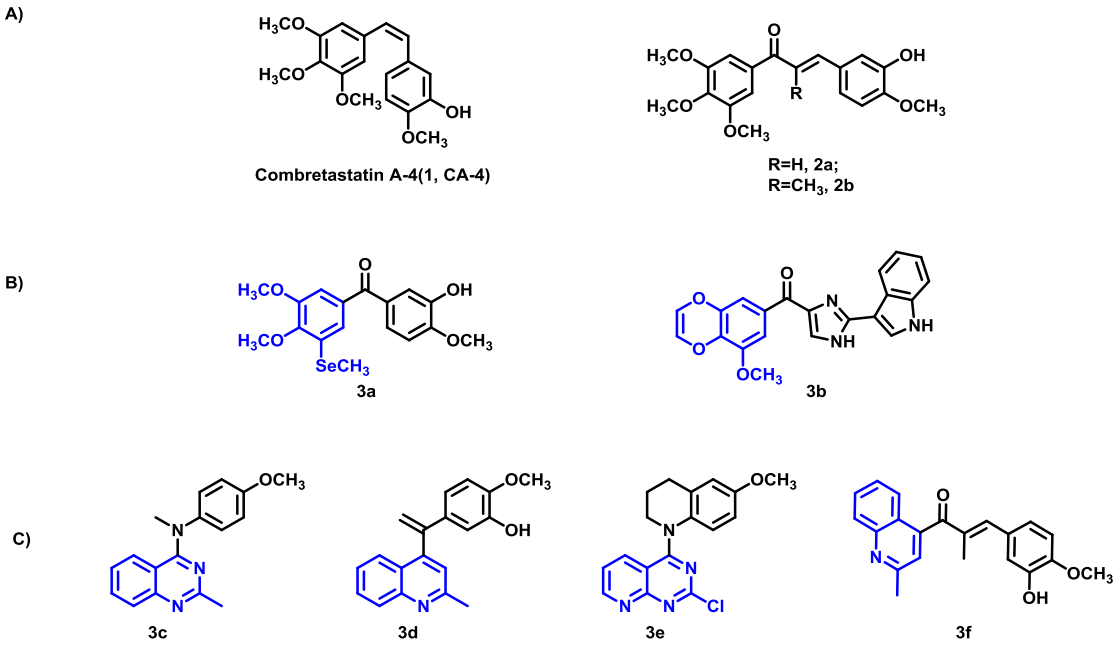

Figure 1. A) Structures of the representative colchicine binding site inhibitors (CBSIs); B) CBSIs reported to modify TMP; C) CBSIs containing nitrogenous heterocycles in replace of TMP.

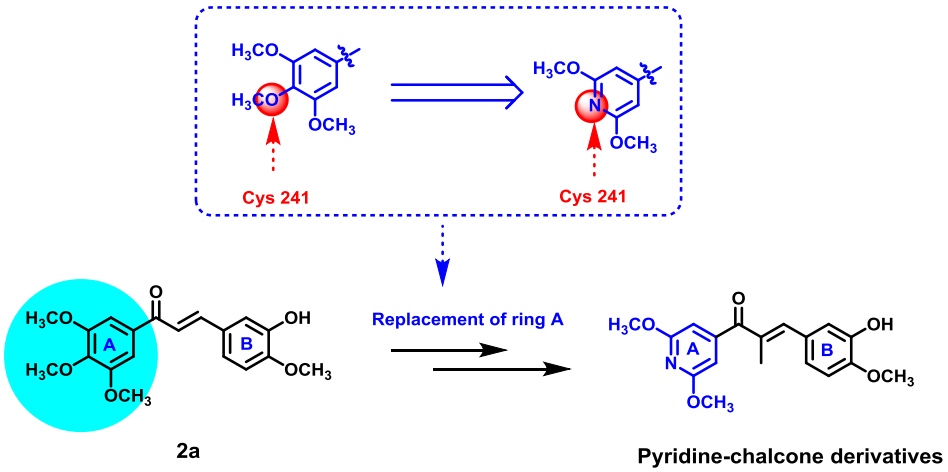

Figure 2. Design strategy of novel pyridine-chalcone derivatives.

2. Results and discussion

2.1 *Chemistry*

The synthetic route for the synthesis of pyridine-chalcone derivatives **15a-f** and **16a-f** is outlined in Scheme 1. The intermediates **9a**, **9b** and **14** are synthesized by two different routes. The starting material 2,6-dichloroisonicotinic acid (**4**) underwent nucleophilic attack by ethylmagnesium bromide (EtMgBr) to give intermediate **5** which was then treated with 2-bromoethanol to give intermediate **6**. Intermediates **7** and **8** were prepared by treating intermediate **6** with sodium methoxide in 60 ℃ and 100 ℃, respectively, followed by deprotection with hydrochloric acid to afford intermediates **9a** and **9b**, respectively. As for intermediate **14**, the starting material 2,6-dichloroisonicotinic acid (**4**) was first treated with *N*-methoxymethanamine to obtain intermediate **10** then underwent nucleophilic attack by methylmagnesium bromide (MeMgBr) to give intermediate **11**. Then the procedures are the same as **9a** and **9b**. Subsequently, ketone **9a**, **9b** and **14** were underwent Aldol reaction with a variety of aldehydes to obtain target compounds **15a-r** and **16a-f**.

Scheme 1. The synthetic route for the preparation of compounds **15a-f** and **16a-f** [a].

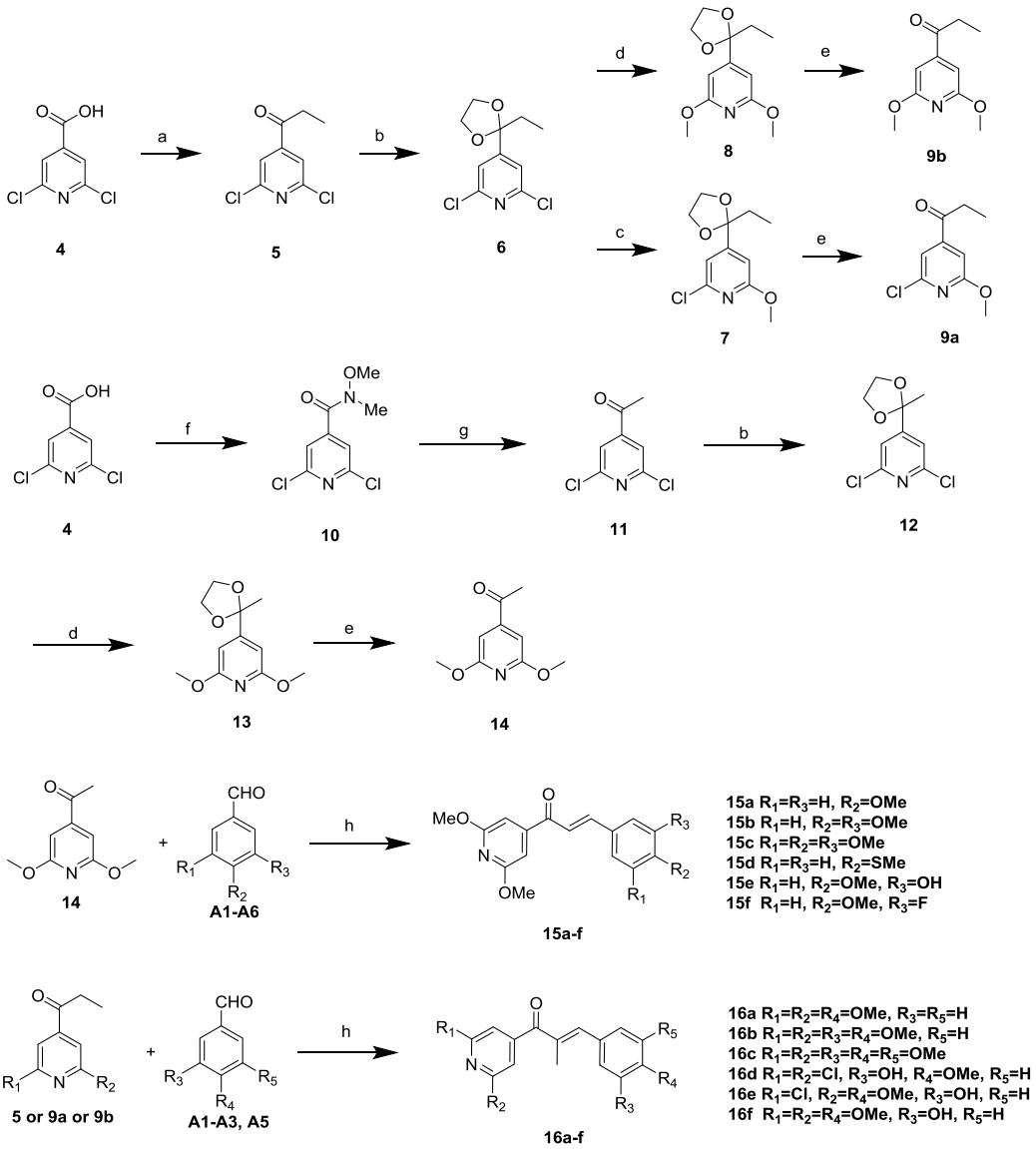

[a] Reagents and conditions: (a) EtMgBr, HCOOEt, THF, N_2, rt, 1 h; (b) $BrCH_2CH_2OH$, DBU, Tol, 80 ℃, overnight; (c) MeONa, MeOH, 60 ℃, overnight; (d) MeONa, MeOH, 100 ℃, overnight; (e) 1M HCl, MeOH, 60 ℃, 1 h; (f) EDCI, HOBt, *N*-methoxymethanamine, Et_3N, DCM, rt, 8 h; (g) CH_3MgBr, THF, N_2, rt, 1 h; (h) NaOH, EtOH, rt, 3 h.

Pyridine-indole derivatives **18a-i** with different substituted positions on the indole ring were synthesized as shown in Scheme 2. Indolealdehyde derivatives were prepared by Vilsmeier-Haack reaction with DMF and phosphoryl chloride. Target compounds **18a-i** were synthesized through Aldol reactions by treating indolealdehyde with ketone **9** in the presence of piperidine.

Scheme 2. The synthetic route for the preparation of compounds **18a-i** [a].

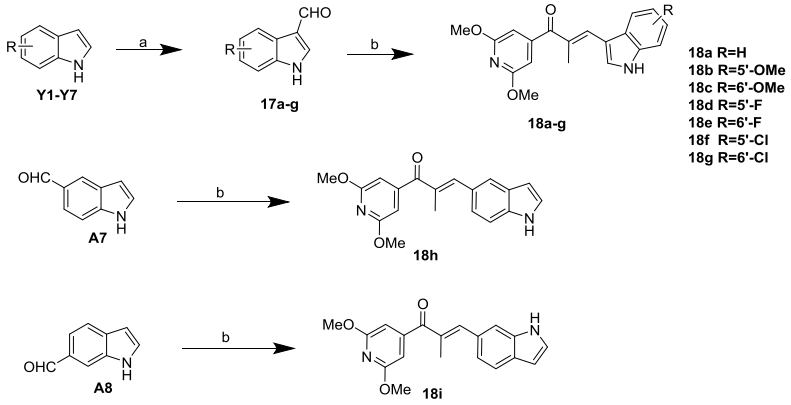

[a] Reagents and conditions: (a) $POCl_3$, DMF, 0 ℃, 10 min; (b) piperidine, EtOH, reflux, overnight.

Compounds **19a-g** were prepared as shown in Scheme 3. The compounds **18a** and **18h** was treated with methyl iodine and ethyl iodine to give the target compounds **19a**, **19b** and **19h**, respectively. And compound **18a** was converted to **19c** using formaldehyde with sodium hydroxide under refluxing condition. Also, compound **18a** was reacted with acetyl chloride, 2-furoyl chloride and benzoyl chloride to provide the corresponding compounds **19d-f**.

Scheme 3. The synthetic route for the preparation of compounds **18a-g** [a].

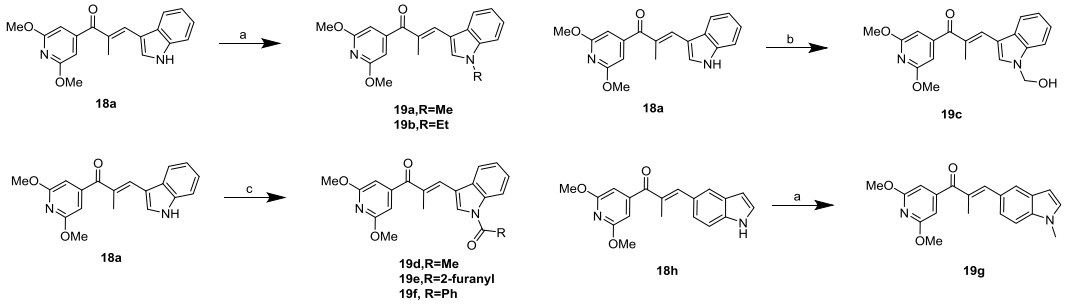

[a] Reagents and conditions: (a) NaH, MeI, DMF, 0 ℃, 1 h; (b) HCHO, EtOH, NaOH, reflux, 1 h; (c) acyl chloride, NaOH, DCM, rt, 2 h.

2.2 In vitro antiproliferative activity

Target compounds **15a-f, 16a-f, 18a-i** and **19a-g** were evaluated for their *in vitro* antiproliferative efficacy against K562 cells by the MTT assays with CA-4 as the reference. As shown in Table 1, compounds with indole moieties as ring B showed favorable activity except **18b**, **18f**, **18h** and **19b**. Compound **16f** that bear

3-hydroxy-4-methoylphenyl moiety displayed the most potent activity with the IC_{50} value of 0.023 μM, which was about 3-fold increase in activity when compared with the parent compound **2a** (IC_{50} = 0.068 μM), and was slightly less potent than the CA-4 (IC_{50} = 0.011 μM). The methyl substituted at the α-position of unsaturated carbonyl group was favorable for the improvement of activity (**15a** *vs* **16a**, **15b** *vs* **16b**, **15c** *vs* **16c** and **15e** *vs* **16f**), which was accordance with the results in the previous reports [7]. Besides, the exposed hydroxyl on ring B was essential for maintaining the activity (**16b** *vs* **16f**). Moreover, the substituents on the pyridine were also critical to the activity (**16d**, **16e** and **16f**), indicating that the electron-donating groups (EDG) were more favorable than the electron-withdraw groups (EWG). We proposed that the EDG increased the electron density of the *N*-1 of pyridine, which was beneficial to form a hydrogen bond with the critical residue Cys241. Also, the results indicated that the 3-substitued indoles were more favorable (**18a** *vs* **18h** and **18i**), and while substituents at N-1 of indole ring were unfavorable to activity (**18a** *vs* **18b-g**, **18a** *vs* **19a-f**).

Table 1. Antiproliferative activities of compounds **15a-f, 16a-f, 18a-g** and **19a-g** against K562 cell line [a].

Compd.	IC_{50} values (μM)[b]	Compd.	IC_{50} values (μM)[b]
	K562		K562
15a	> 1	**18d**	0.352 ± 0.004
15b	> 1	**18e**	0.191 ± 0.008
15c	> 1	**18f**	> 1
15d	> 1	**18g**	0.106 ± 0.006
15e	0.983 ± 0.013	**18h**	> 1
15f	> 1	**18i**	0.142 ± 0.036
16a	0.554 ± 0.017	**19a**	0.700 ± 0.023
16b	> 1	**19b**	> 1
16c	> 1	**19c**	0.058 ± 0.006
16d	0.156 ± 0.012	**19d**	0.086 ± 0.008
16e	0.138 ± 0.011	**19e**	0.060 ± 0.003
16f	0.023 ± 0.002	**19f**	0.070 ± 0.003
18a	0.051 ± 0.003	**19g**	0.952 ± 0.017
18b	> 1	**2a**	0.068± 0.002
18c	0.983 ± 0.018	**CA-4**	0.011 ± 0.001

[a] Cells were treated with different concentrations of the compounds for 72 h. Cell viability was measured by the

MTT assay as described in the Experimental Section.

[b] IC_{50} values are indicated as the mean ± SD (standard error) of at least three independent experiments.

Table 2. Antiproliferative activities of representative compounds against five cancer cell lines and one normal cell line [a]

Compd.	IC_{50} values (μM)[b]					
	HepG2	KB	HCT-8	MDA-MB-231	H22	L-O2
15e	0.991 ± 0.021	1.018 ± 0.015	0.997 ± 0.010	1.128 ± 0.011	0.928 ± 0.065	4.226 ± 0.321
16d	0.183 ± 0.008	0.162 ± 0.003	0.177 ± 0.005	0.195 ± 0.009	0.177 ± 0.011	0.399 ± 0.031
16e	0.132 ± 0.010	0.147 ± 0.012	0.139 ± 0.012	0.162 ± 0.013	0.142 ± 0.014	0.768 ± 0.054
16f	0.047 ± 0.002	0.045 ± 0.001	0.047 ± 0.003	0.041 ± 0.004	0.043 ± 0.002	0.157 ± 0.013
18a	0.085 ± 0.005	0.090 ± 0.003	0.095 ± 0.003	0.079 ± 0.002	0.088 ± 0.012	0.408 ± 0.036
18d	0.392 ± 0.009	0.324 ± 0.013	0.335 ± 0.011	0.320 ± 0.016	0.336 ± 0.025	1.271 ± 0.121
18e	0.364 ± 0.012	0.421 ± 0.022	0.379 ± 0.018	0.364 ± 0.015	0.428 ± 0.041	1.102 ± 0.104
18g	0.124 ± 0.012	0.137 ± 0.013	0.127 ± 0.010	0.153 ± 0.014	0.127 ± 0.013	0.628 ± 0.057
18i	0.157 ± 0.003	0.143 ± 0.008	0.152 ± 0.006	0.148 ± 0.005	0.138 ± 0.008	0.728 ± 0.069
19c	0.092 ± 0.003	0.109 ± 0.006	0.121 ± 0.009	0.088 ± 0.007	0.098 ± 0.007	0.417± 0.032
19e	0.068 ± 0.002	0.072 ± 0.006	0.091 ± 0.008	0.082 ± 0.008	0.075 ± 0.002	0.338 ± 0.031
19f	0.093 ± 0.001	0.107 ± 0.001	0.110 ± 0.003	0.093 ± 0.007	0.108 ± 0.011	0.528 ± 0.042
2a	0.102± 0.010	0.108 ± 0.005	0.104 ± 0.010	0.102 ± 0.009	0.132 ± 0.008	0.421 ± 0.037
CA-4	0.012± 0.001	0.011 ± 0.002	0.010 ± 0.001	0.010 ± 0.001	0.008 ± 0.001	0.095 ± 0.011

[a] Cells were treated with different concentrations of the compounds for 72 h. Cell viability was measured by the MTT assay as described in the Experimental Section.

[b] IC_{50} values are indicated as the mean ± SD (standard error) of at least three independent experiments.

In consideration of the prominent antiproliferative activities of the newly pyridine-chalcone derivatives against K562 cells, we tend to further evaluate the biological functions against more cancer cell lines. Human hepatocellular carcinoma (HepG2), epidermoid carcinoma of the nasopharynx (KB), human ileocecal cancer cells (HCT-8) human breast cancer cells (MDA-MB-231), and hepatoma 22 cells (H22) were selected for the further evaluation of activity. In addition, one normal non-cancerous cell line - human normal liver cells (L-O2) - was chosen to evaluate the toxicity of these compounds. The cytotoxic data of representative compounds

against these four cancer cell lines were shown in Table 2, which showed that all these chosen compounds displayed potent activities against these four cancer cell lines. Moreover, the structure activity relationships (SARs) were similar to their performances in K562 assays. Also, the K562 cell was the most sensitive cell line among five cancer cell lines tested, and the most active compound **16f** exhibited remarkable activity with IC_{50} values ranging from 0.023 to 0.047 μM, which was about 3-fold improvement of activity when compared with the parent compound **2a**. The SARs of synthesized compounds were summarized in Figure 3.

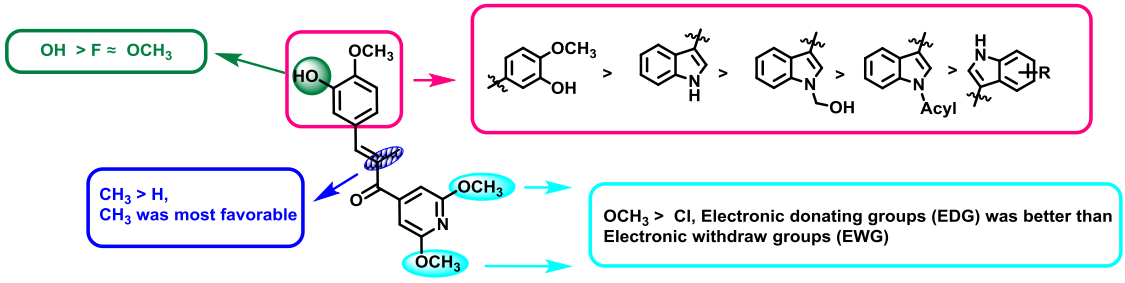

Figure 3. Summarized SARs of synthesized compounds.

2.3 In vitro tubulin polymerization inhibitory assay

To verify whether the target molecules interacted with microtubule systems, **16f**, the most cytotoxic compounds, was selected for the experiment of effects on microtubule dynamics. Also colchicine（a typical microtubule-destabilizing agent）and taxol (microtubule-stabilizing agent) were chosen as the controls. As shown in Figure 4, the fluorescence emission of **16f** was less than the control group and similar to the colchicine group, indicating that **16f** was a microtubule-destabilizing agent. Moreover, the calculated IC_{50} value of **16f** in inhibiting tubulin polymerization was 2.08 μM, which was better than the CA-4 (IC_{50} = 2.17 μM) and the parent compound **2a** (IC_{50} =3.05 μM) (Table 3). In addition, the test of competing with [3H]-colchicine in binding to tubulin was performed, indicating that **16f** bound to the colchicine binding site with the potency about 87.9% at 5 μM, (Table 3). Hence, **16f** was chosen

for further mechanism studies due to its excellent activities both in the *in vitro* antiproliferative assay and tubulin polymerization inhibition assay.

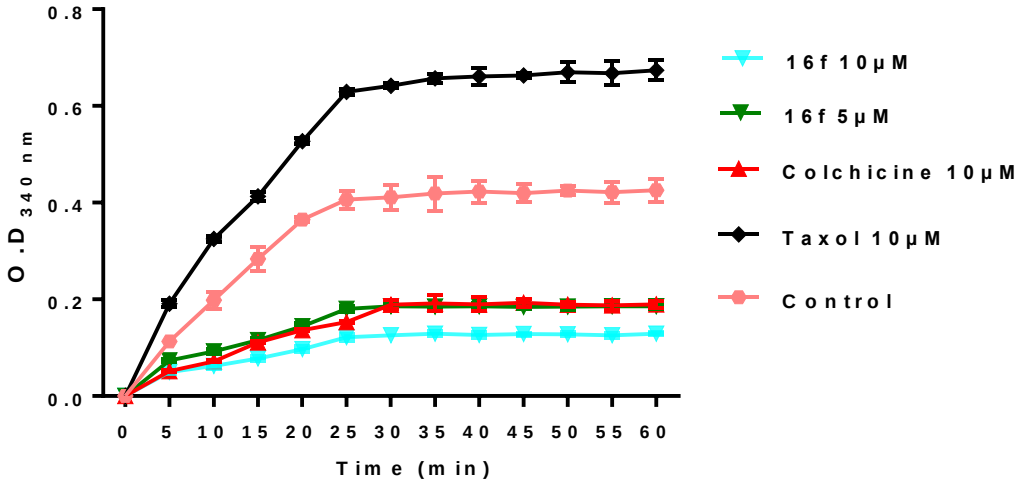

Figure 4. Effects of **16f** on tubulin polymerization *in vitro*. Purified tubulin protein at 2 mg/mL in a reaction buffer was incubated at 37 °C in the presence of 1% DMSO, test compounds (**16f** at 5 or 10 μM), Colchicine (10 μM) or Taxol (10 μM). Polymerizations were followed by an increase in fluorescence emission at 350 nm over a 60 min period at 37 °C. The experiments were performed three times.

Table 3. Inhibition of tubulin polymerization[a] and colchicine binding to tubulin[b]

Compd.	inhibition of tubulin polymerization	inhibition of colchicine binding (%) inhibition ± SD	
	IC_{50} (μM)	1 μM	5 μM
16f	2.08 ± 0.12	75.1 ± 1.63	87.9 ± 2.18
CA-4	2.17 ± 0.14	81.2 ± 2.01	91.7 ± 4.40
2a	3.05 ± 0.15	70.2 ± 1.71	78.3 ± 3.39

[a] The tubulin assembly assay measured the extent of assembly of 2 mg/mL tubulin after 60 min at 37 °C. Data are presented as mean from three independent experiments.

[b] Tubulin, 1 μM; [3H]-colchicine, 5 μM; and inhibitors, 1 or 5 μM.

2.4. Anti-microtubule effects in K562 cells

Immunofluorescent assay was performed to investigate the effects of compound **16f** on microtubule networks. As shown in Figure 5, K562 cells and MAD-MB-231

cells without drug treatment exhibited normal filamentous arrays. However, after exposure to **16f** (10 nM, 20 nM, 40 nM to K562, and 20 nM, 40 nM, 80 nM to MAD-MB-231) for 24 h, the microtubule networks in cytosol were disrupted; these results indicated that **16f** can induce a dose-dependent collapse of the microtubule networks.

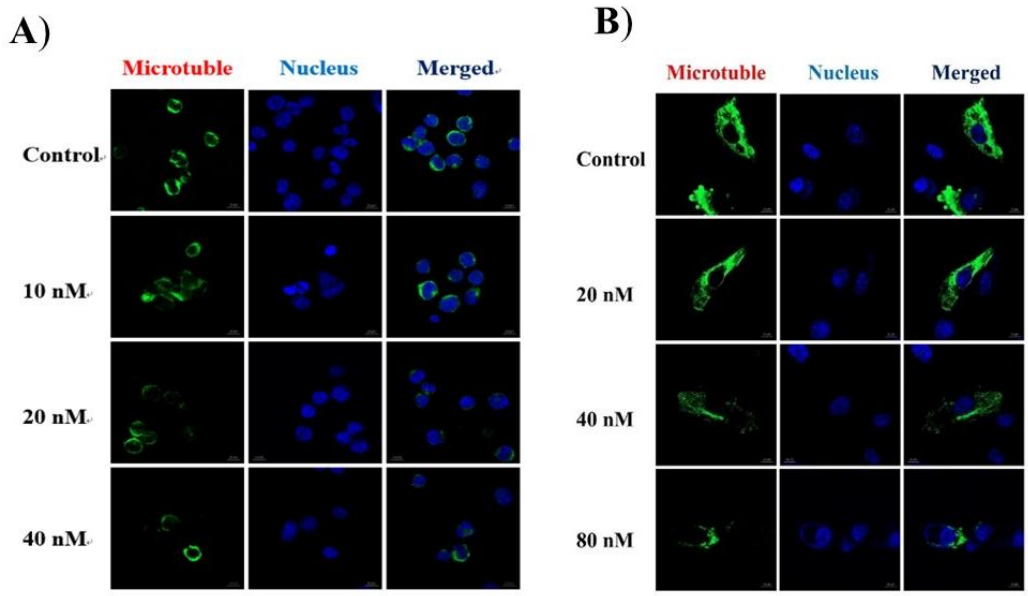

Figure 5. A) Effects of **16f** on the cellular microtubule network visualized by immunofluorescence. K562 cells were treated with vehicle control 0.1% DMSO, **16f** (10 nM), **16f** (20 nM), and **16f** (40 nM). B) Effects of **16f** on the cellular microtubule network visualized by immunofluorescence. MAD-MB-231 cells were treated with vehicle control 0.1% DMSO, **16f** (20 nM), **16f** (40 nM), and **16f** (80 nM).Then, the cells were fixed and stained with anti-α-tubulin-FITC antibody (green), Alexa Fluor 488 dye and counterstained with DAPI (blue). The detection of the fixed and stained cells was performed with an LSM 570 laser confocal microscope (Carl Zeiss, Germany).

2.5 Cell cycle analysis

Since most microtubule polymerization inhibitors disrupt cell mitosis and exert cell cycle arrest effects, the effect of **16f** on cell cycle progression using propidiumiodide (PI) staining in K562 cells was examined. As illustrated in Figure 6A and 6B, incubation with **16f** blocked the cell cycle at the G2/M phase. Compared to the

control cells incubated with DMSO, the incubation of K562 cells with increasing concentrations of **16f** (15, 30, and 60 nM) increased the percentage of cells in the G2/M phase from 7.10% to 33.22%.

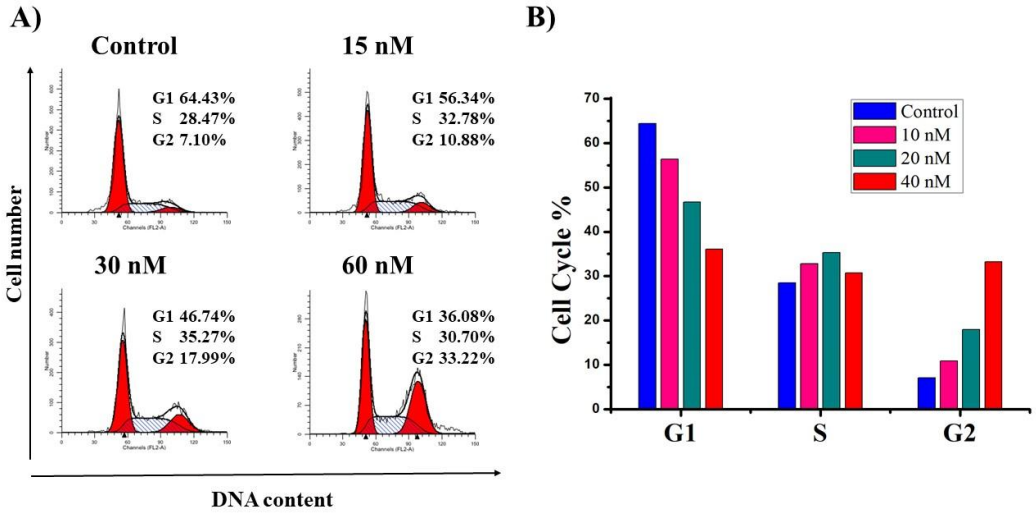

Figure 6. A) Compound **16f** induced G2/M arrest in K562 cells. K562 cells were incubated with varying concentrations of **16f** (0, 15, 30, and 60 nM) for 48 h. Cells were harvested and stained with PI and then analyzed by flow cytometry. The percentages of cells in different phases of the cell cycle were analyzed by ModFit 4.1; B) Histograms display the percentage of cell cycle distribution after treatment with **16f**.

2.6 Cell apoptosis analysis

Most microtubule polymerization inhibitors can induce cell apoptosis by up-regulating the expression of pro-apoptotic proteins and down-regulating the expression of antiapoptotic proteins. Aiming to assess whether compound **16f** would induce cell apoptosis, an annexin VFITC and propidium iodide (PI) assay was carried out. As shown in Figure 7A and 7B, the percentage of apoptotic cells after the 48 h treatment was only 3.42% in the control group, but the total numbers of early (annexin-V^+/PI^-) and late (annexin-V^+/PI^+) apoptotic cells increased to 15.79%, 39.01% and 56.07% after treatment with **16f** at 10, 20, and 40 nM for 48 h, respectively. These results confirmed that compound **16f** effectively induced cell apoptosis in K562 cells

in a dose-dependent manner.

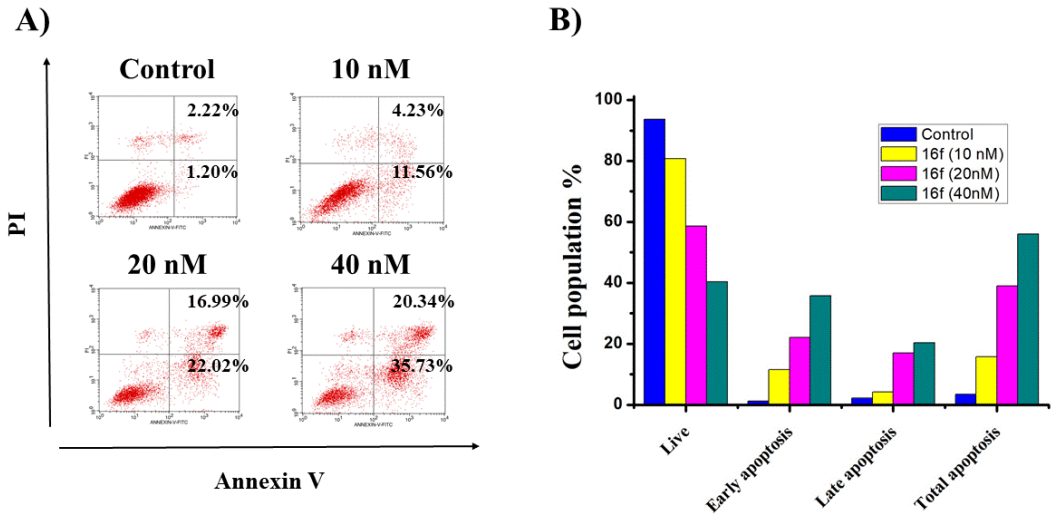

Figure 7. A) Compound **16f** induced apoptosis in K562 cells. K562 cells were incubated with varying concentrations of **16f** (0, 10, 20, and 40 nM). After 48 h of incubation, cells were collected and stained with Annexin V/PI, followed by flow cytometric analysis. The percentages of cells in each stage of cell apoptosis were quantified by flow cytometry: (upper left quadrant) necrosis cells; (upper right quadrant) late-apoptotic cells; (bottom left quadrant) live cells; and (bottom right quadrant) early apoptotic cells. B) Histograms display the percentage of cell distribution after treatment with **16f**.

2.7 Mitochondrial membrane potential analysis.

Decreased mitochondrial membrane potential (MMP) has been implicated as an early event in apoptotic cells. Thus, the effect of compound **16f** on MMP of K562 cells was determined by staining with lipophilic cationic JC-1 dye. When treated with **16f** at concentrations of 0, 10, 20 and 40 nM for 24 h, the number of K562 cells with collapsed MMP increased to 5.75%, 16.44%, 28.10% and 44.49%, respectively. (Figure 8), suggesting that **16f** caused mitochondrial depolarization of K562 cells in the process of apoptosis.

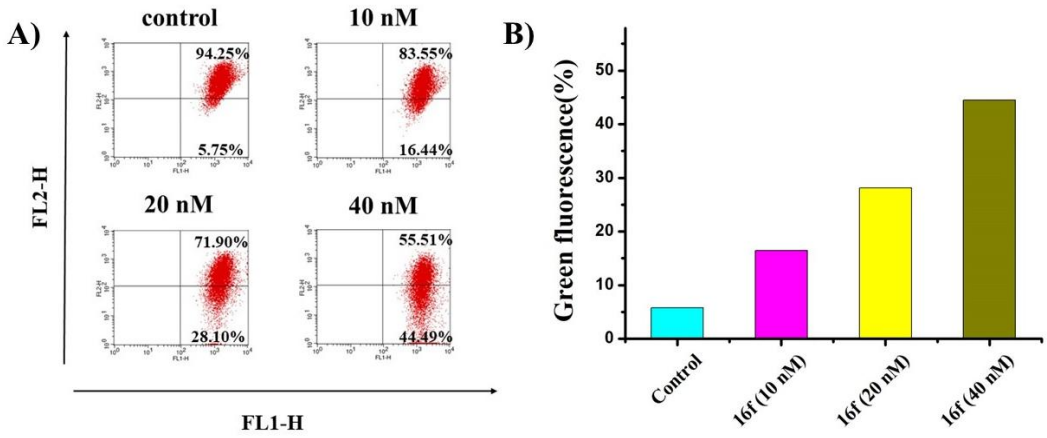

Figure 8. Effects of **16f** on the mitochondrial membrane potential of K562 cells. A) Incubation with different concentrations (0, 10, 20, and 40 nM) of **16f** in K562 cells for 24 h prior to staining with JC-1 dye, the number of cells with collapsed mitochondrial membrane potentials was determined by flow cytometry analysis. B) Histograms display the percentage of green fluorescence.

2.8 In vitro evaluation of anti-vascular activity

In view of such facts that most CBSIs possess vascular disrupting activity, we further evaluated the anti-vascular activity of compound **16f**. The HUVECs culture assays were performed to assess the ability of **16f** to inhibit HUVECs migration which is the key step to generate new blood vessels. As shown in Figure 9A, the untreated cells migrated to fill the area that was initially scraped after 24 h. In contrast, **16f** significantly inhibited the HUVEC migration in a dose-dependent manner.

Then we further assessed the anti-vascular activity of **16f** in a tube formation assay. After being seeded on Matrigel, HUVECs formed the capillary-like tubules with multicentric junctions. After exposure to **16f** at 10, 20, and 40 nM for 6 h, the capillary-like tubes were interrupted in different levels (Figure 9B). These results showed that compound **16f** effectively has an effect on tubule-like disruption of HUVECs.

The antiproliferative activity of **16f** against HUVECs was also determined by an MTT assay to exclude the possibility that the anti-vascular activity of **16f** was due to a

cytotoxic action of **16f**. The calculated IC_{50} value of **16f** against HUVECs after a 24 h treatment was 0.126 ± 0.007 μM, which is higher than the concentration of 40 nM required for the obvious inhibition of cell migration and tube formation. These results indicate that **16f** exhibited anti-vascular activity.

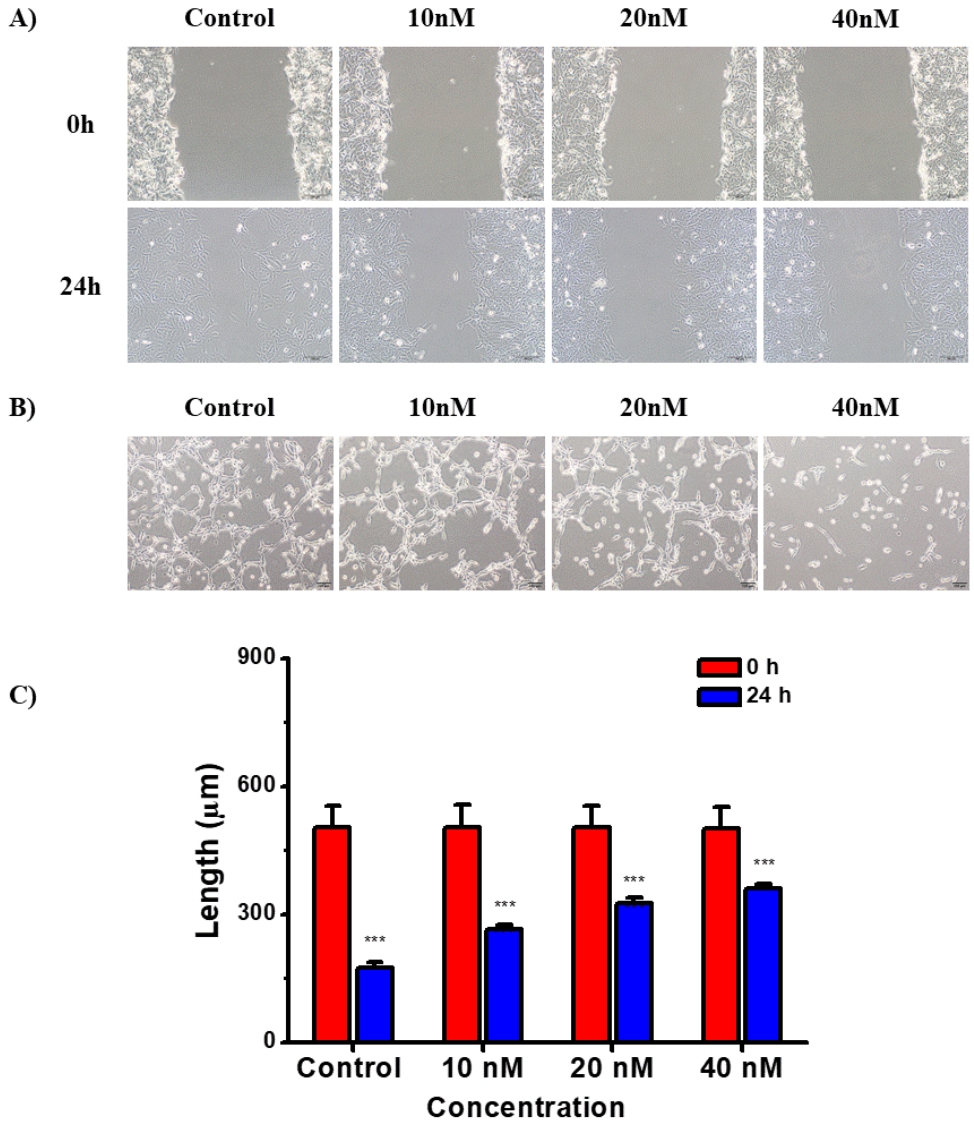

Figure 9. Effects on the HUVECs migration and tube formation. A) Scratches were created with sterile 200 μL pipette and images were captured using phase contrast microscopy at 0 h and 24 h after treatments with 0, 10, 20 and 40 nM of **16f**. B) Images depicting the formation of HUVEC capillary-like tubular network by treatments with 0, 10, 20 and 40 nM of **16f** for 6 h. C) Histograms display the length of the scratches at 0 h and 24 h after treatments with 0, 10, 20 and 40 nM of **16f**, ***, $P < 0.001$ *vs* control group.

*2.9 In vivo antitumor activity of **16f***

To evaluate the *in vivo* antitumor activities of **16f**, liver cancer allograft mouse model was established by subcutaneous inoculation of H22 cells into the right flank of mice. The tumor size and body weights of the mice were monitored and recorded every 2 days. Paclitaxel (PTX), CA-4 and the disodium phosphate of CA-4 (CA-4P) were selected as the positive controls. As shown in Figure 10A and Figure 10B, **16f** at the dose of 20 mg/kg per day significantly decreased the tumor volume. Obviously, the reduction in tumor weight reached 65.8% at dose of 20 mg/kg per day (i.v.) of **16f**, which was slightly less potent than PTX (72.7% at a dose of 6 mg/kg per 2 days). Particularly, **16f** at the dose of 20 mg/kg displayed more potent antitumor activity than CA-4 (inhibition rate: 50.9% at 20 mg/kg) or CA-4P (inhibition rate: 62.7% at 20 mg/kg) (Figure 10D). Moreover, **16f** did not significantly affected body weight even at the doses of 20 mg/kg, while treatment with PTX at a dose of 6 mg/kg per 2 days led to a significant influence on body weight (Figure 10C). Thus, compound **16f** is worthy of further investigation for the treatment of cancers.

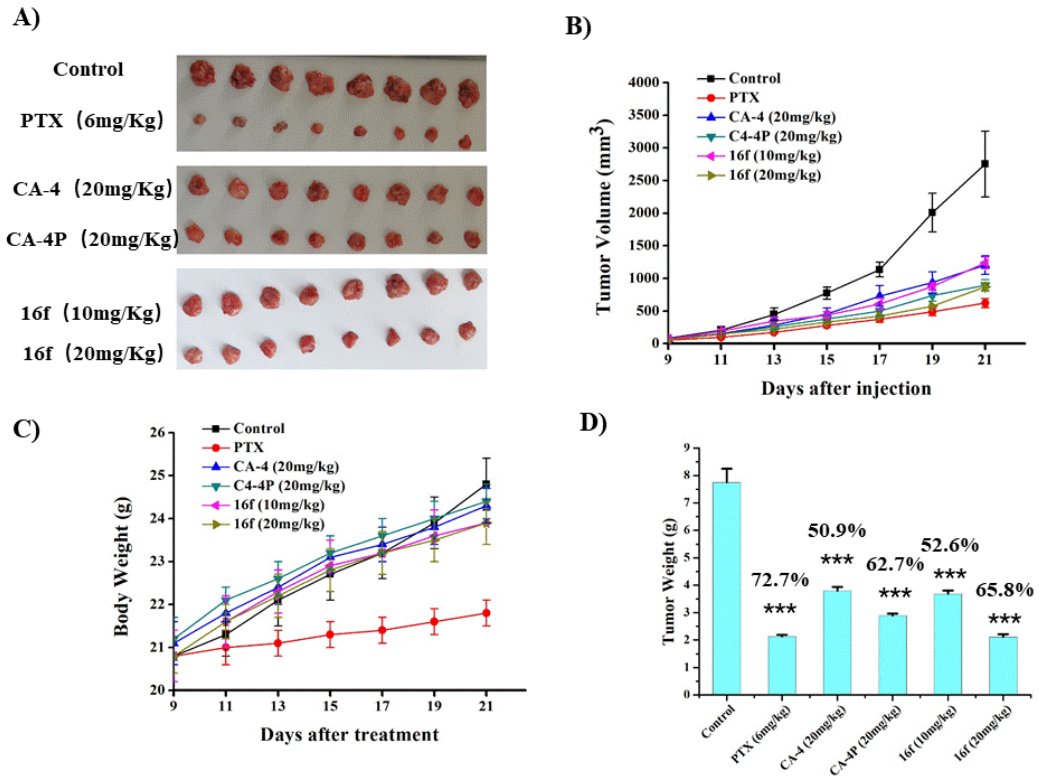

Figure 10. **16f** inhibited liver cancer allograft growth *in vivo*. After administered with vehicle, PTX (6 mg/kg per 2 days, group 2), CA-4 (20 mg/kg per day), CA-4P (20 mg/kg per day), **16f** (10 mg/kg per day), and **16f** (20 mg/kg per day) for three weeks, the mice were sacrificed, and the tumors were weighed. A) The images of tumors from mice at 21 days after initiation of treatment. B) Tumor volume changes of mice during treatment. C) Body weight changes of mice during treatment. D) The weight of the excised tumors of each group. $^{**}P < 0.05$, $^{***}P < 0.001$ *vs* control group.

2.10 Molecular modelling studies

To explain the binding modes of the most active compound **16f** with tubulin, we performed a docking study of **16f** into the colchicine binding pocket of tubulin (PDB: 5lyj) by using the DOCK program in the Discovery Studio 3.0 software. As shown in figure 11A, **16f** adopted a very similar positioning to the colchicine at the colchicine binding pocket. As displayed in figure 11B, the *N*-1 of pyridine moiety formed a critical hydrogen bond with residue Cys241 resembling that of the 4-methoxy group in compound **2a**. Moreover, the hydroxy group of ring B formed two additional

hydrogen bonds with Val181 and Asn258, which illustrated the vital role of the exposed hydroxyl group.

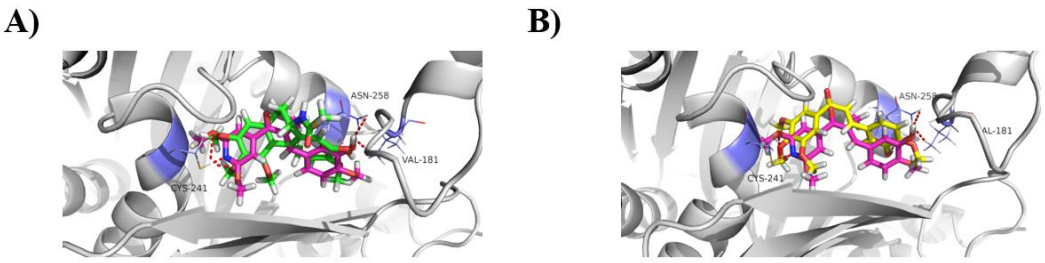

Figure 11. Proposed binding model for **16f** (violet) binding with tubulin (PDB code: 5lyj), and overlapping with colchicine (green) and compound **2a** (yellow).

3. Conclusion

In summary, we designed and synthesized a series of novel pyridine-chalcone derivatives as microtubule destabilizing agents, which may have some potential advantages over the reported chalcones.

All compounds were evaluated for their anti-proliferative activities, and their detailed SARs were obtained. Compound **16f** exhibited the most potent activities against five cancer cell lines with IC_{50} values ranging from 23 to 45 nM, which was 3-fold more potent than parent compound **2a**. Compared to chalcone derivatives without nitrogenous heterocycles, such as **2a** and **2b**, the introduction of pyridine moiety, which can be further prepared as the hydrochloride salts, provides an alternative method to improve the solubility of CBSIs. On the other hand, compound **16f** has a promising application in development for its simpler processing than that of the quinoline-chalcone derivatives in our previous study [20].

Besides, by using colchicine competition inhibition assay and molecular modelling studies, representative compound **16f** was verified to bind to the colchicine binding site as microtubule-destabilizing agent with the IC_{50} value of 2.08 μM. Further mechanism studies demonstrated that **16f** disrupted microtubule networks, arrested cell cycle at G2/M phase, induced apoptosis and depolarized mitochondria of

K562 cells in a dose-dependent manner. Furthermore, the wound healing and tube formation assays also identified **16f** as a novel vascular disrupting agent. The most importantly, the *in vivo* antitumor experiments displayed that **16f** effectively suppressed the tumor volume and reduced tumor weight by 65.8% at the dose of 20 mg/kg per day (i.v.), which was more potent than control compound CA-4 (inhibition rate: 50.9% at 20 mg/kg) or CA-4P (inhibition rate: 62.7% at 20 mg/kg). Collectively, the present study demonstrates that pyridine-chalcone derivative **16f** represents a novel class of anti-tubulin agent with potent anti-vascular and antitumor activities and deserves further investigation.

EXPERIMENTAL SECTION

4.1. Chemistry

4.1.1. General

Most chemicals and solvents were purchased from commercial sources. Further purification and drying by standard methods were employed when necessary. ^{1}H NMR and ^{13}C NMR spectra were recorded on Bruker-300 spectrometers in the indicated solvents (TMS as internal standard). Data are reported as follows: chemical shift in ppm (d), multiplicity (s =singlet, d =doublet, t =triplet, q =quartet, brs = broad singlet, m =multiplet), coupling constant (Hz), and integration. High Resolution Mass measurement was performed on Agilent QTOF 6520 mass spectrometer with electron spray ionization (ESI) as the ion source. Flash column chromatography was carried out using commercially available silica gel (200-300 mesh) under pressure.

*4.1.2 Synthesis of intermediate **5***

To a solution of 2,6-dichloroisonicotinic acid (10 g, 52 mmol) in 50 mL anhydrous THF under nitrogen atmosphere at 0 °C was added C_2H_5MgBr in diethyl ether (2 M, 80 mL, 160 mmol). After stirring for 2 h, the reaction was quenched by NH_4Cl aqueous, and extracted with CH_2Cl_2 (3 × 50 mL). The combined organic layers were then washed with brine, dried over anhydrous Na_2SO_4, and concentrated in vacuo to

provide the crude product, which was purified by column chromatography with petroleum/ethyl acetate (4:1) to give intermediate **5** as white solid (9.0 g, 85.1 %).^{1}H NMR (300 MHz, $CDCl_3$) δ 7.67 (s, 2H), 2.96 (q, *J* = 7.1 Hz, 2H), 1.22 (t, *J* = 7.1 Hz, 3H), ^{13}C NMR (75 MHz, $CDCl_3$) δ 197.15, 151.85, 147.70, 120.91, 32.64, 7.54; ESI-MS *m/z*: 202.9 $[M+Na]^+$ 225.9.

4.1.3 Synthesis of intermediate ***6***

To a solution of **5** (6 g, 29.4 mmol) in anhydrous toluene was added DBU (12.43 mL, 88.2 mmol), 2-bromoethanol (10.42 mL, 147 mmol). The mixture was stirred at 80 °C overnight. Then the solvent was removed in vacuo, and the residue was diluted by H_2O, and extracted with CH_2Cl_2 (3 × 20 mL). The combined organic layers were then washed with brine, dried over anhydrous Na_2SO_4, and concentrated in vacuo to provide the crude product, which was purified by column chromatography with petroleum/ethyl acetate (40:1) to give intermediate **6** as colorless oil (6 g, 83.2 %).^{1}H NMR (300 MHz, $CDCl_3$) δ 7.33 (s, 2H), 4.05 (t, *J* = 6.8 Hz, 2H), 3.78 (t, *J* = 6.9 Hz, 2H), 1.85 (q, *J* = 7.6 Hz, 2H), 0.89 (t, *J* = 7.4 Hz, 3H); ESI-MS *m/z*: 247.0 $[M+Na]^+$ 270.0.

4.1.4 Synthesis of intermediate ***9a***

To a solution of **6** (2.5 g, 10.1 mmol) in anhydrous MeOH was added sodium methoxide solid (5.45 g, 101 mmol). The mixture was stirred at 60 °C in sealed tube overnight. Then the reaction was quenched by H_2O, the solvent was removed in vacuo, and the residue was extracted with CH_2Cl_2 (3 × 20 mL). The combined organic layers were then washed with brine, dried over anhydrous Na_2SO_4, and concentrated in vacuo to provide the crude product, which was dissolved in MeOH, and concentrated hydrochloric acid (10 mL) was added. Then the mixture was stirred at room temperature for 2 h. Then, the solution was neutralized with 2 M NaOH aqueous to pH 7, and extracted with CH_2Cl_2 (3 × 20 mL). The combined organic layers were then washed with brine, dried over anhydrous Na_2SO_4, and concentrated in vacuo to provide the crude product, which was purified by column chromatography with petroleum/ethyl acetate (4:1) to give intermediate **9a** as yellow solid (1.5 g, 79.1%).^{1}H NMR (300 MHz, $CDCl_3$) δ 7.33 (s, 1H), 7.09 (s, 1H), 3.98 (s, 3H), 2.93 (q, *J* = 7.1 Hz,

2H), 1.25 - 1.17 (m, 3H); ESI-MS *m/z*: 199.0 $[M+Na]^+$ 222.0.

4.1.5 Synthesis of intermediate ***9b***

To a solution of **6** (5 g, 20.2 mmol) in anhydrous MeOH was added sodium methoxide solid (10.89 g, 202 mmol). The mixture was stirred at 100 °C in sealed tube overnight. Then the reaction was quenched by H_2O, the solvent was removed in vacuo, and the residue was extracted with CH_2Cl_2 (3 × 20 mL). The combined organic layers were then washed with brine, dried over anhydrous Na_2SO_4, and concentrated in vacuo to provide the crude product, which was dissolved in MeOH, and concentrated hydrochloric acid (10 mL) was added. Then the mixture was stirred at room temperature for 2 h. Then, the solution was neutralized with 2 M NaOH aqueous to pH 7, and extracted with CH_2Cl_2 (3 × 20 mL). The combined organic layers were then washed with brine, dried over anhydrous Na_2SO_4, and concentrated in vacuo to provide the crude product, which was purified by column chromatography with petroleum/ethyl acetate (4:1) to give intermediate **9b** as yellow solid (3.2 g, 81.1 %).^{1}H NMR (300 MHz, CDCl3) δ 6.75 (s, 2H), 3.95 (s, 6H), 2.92 (q, *J* = 6.5 Hz, 2H), 1.20 (t, *J* = 7.4 Hz, 3H). ^{13}C NMR (75 MHz, $CDCl_3$) δ 200.01, 164.01, 148.70, 99.41, 53.89, 32.44, 7.85; ESI-MS *m/z*: 195.0 $[M+Na]^+$ 218.0.

4.1.6 Synthesis of intermediate ***10***

To a solution of **6** (1.5 g, 4.1 mmo) in anhydrous DCM was added HOBt (1.3 g, 4.8 mmol), EDCI (1.8 g, 4.8 mmol), Et_3N (0.62 g, 6.15 mmol) and *N*-methoxymethanamine (1.2 g, 6.6 mmol). The mixture was stirred at room temperature for 2 h. The precipitate was filtered and the filtrate was removed under vacuum. The resulting mixture was then purified by flash column chromatography with petroleum/ethyl acetate (4:1) to give intermediate **10** as white solid (1.6 g, 85.1 %). ^{1}H NMR (300 MHz, $CDCl_3$) δ 7.50 (s, 2H), 3.58 (s, 3H), 3.37 (s, 3H); ESI-MS *m/z*: 233.9 $[M+Na]^+$ 256.9.

4.1.7 Synthesis of intermediate ***11***

To a solution of **10** (1.1 g, 4.68 mmol) in 10 ml anhydrous THF under nitrogen atmosphere at 0 °C was added CH_3MgBr in diethyl ether (3 M, 2.34 mL, 4.80 mmol). After stirring for 2 h, the reaction was quenched by NH_4Cl aqueous, and extracted

with CH_2Cl_2 (3 × 20 mL). The combined organic layers were then washed with brine, dried over anhydrous Na_2SO_4, and concentrated in vacuo to provide the crude product, which was purified by column chromatography with petroleum/ethyl acetate (4:1) to give intermediate **11** as white solid (0.820 g, 92.1 %).^{1}H NMR (300 MHz, $CDCl_3$) δ 7.69 (s, 2H), 2.64 (s, 3H); ESI-MS *m/z*: 188.9 $[M+Na]^+$ 211.9.

*4.1.8 Synthesis of intermediate **14***

To a solution of **11** (1.2 g，6.32 mmol) in anhydrous toluene was added DBU (2.67 mL , 19.0 mmol), 2-bromoethanol (2.24 mL, 31.6 mmol). The mixture was stirred at 80 °C overnight. Then the solvent was removed in vacuo, and the residue was diluted by H_2O, and extracted with CH_2Cl_2 (3 × 20 mL). The combined organic layers were then washed with brine, dried over anhydrous Na_2SO_4, and concentrated in vacuo to provide the crude product **12** as colorless oil (1.25 g, 83.1%). To a solution of **12** (1.25 g, 5.05 mmol) in anhydrous MeOH was added sodium methoxide (2.72 g, 50.5 mmol). The mixture was stirred at 100 °C in sealed tube overnight. Then the reaction was quenched by H_2O, the solvent was removed in vacuo, and the residue was extracted with CH_2Cl_2 (3 × 20 mL). The combined organic layers were then washed with brine, dried over anhydrous Na_2SO_4, and concentrated in vacuo to provide the crude product, which was dissolved in MeOH, and concentrated hydrochloric acid (10 ml) was added. Then the mixture was stirred at room temperature for 2 h. Then, the solution was neutralized with 2 M NaOH aqueous to pH 7, and extracted with CH_2Cl_2 (3 × 20 mL). The combined organic layers were then washed with brine, dried over anhydrous Na_2SO_4, and concentrated in vacuo to provide the crude product, which was purified by column chromatography with petroleum/ethyl acetate (4:1) to give intermediate **14** as white solid (0.8 g, 81.1 %).^{1}H NMR (300 MHz, $CDCl_3$) δ 6.74 (s, 2H), 3.95 (s, 6H), 2.55 (s, 3H), ^{13}C NMR (75 MHz, $CDCl_3$) δ 212.48, 164.06, 148.74, 99.70, 53.94, 27.01; ESI-MS *m/z*: 181.0 $[M+Na]^+$ 204.

*4.1.9 The procedure for the preparation of **15a-f** and **16a-f**.*

To a stirred solution of ketone (0.28 mmol) and aldehyde (0.28 mmol) in anhydrous EtOH, NaOH (55.1 mg, 1.38 mmol) was slowly added at room temperature. After stirring for 3 h, the reaction mixture was concentrated and extracted with CH_2Cl_2 (3 ×

20 mL). The combined organic layers were then washed with brine, dried over anhydrous Na_2SO_4, and concentrated in vacuo to provide the crude product, which was purified by column chromatography with petroleum/ethyl acetate (4:1) to give the corresponding pure compounds ***15a-f*** *and* ***16a-f***.

4.1.9.1 (E)-1-(2,6-dimethoxypyridin-4-yl)-3-(4-methoxyphenyl)prop-2-en-1-one (**15a**). Yellow solid, yield 76.2%. ^{1}H NMR (300 MHz, $CDCl_3$) δ 7.63 (d, *J* = 15.7 Hz, 1H), 7.45 (d, *J* = 8.6 Hz, 2H), 7.07 (d, *J* = 15.7 Hz, 1H), 6.81 (d, *J* = 8.6 Hz, 2H), 6.64 (s, 2H), 3.84 (s, 6H), 3.73 (s, 3H), ^{13}C NMR (75 MHz, $CDCl_3$) δ 189.92, 163.88, 162.04, 150.74, 146.20, 130.47, 127.21, 119.61, 114.50, 99.85, 55.43, 53.89; HR-MS (ESI) *m/z*: calcd for $C_{17}H_{18}NO_4$ $[M+H]^+$ 300.1230 found 300.1229.

4.1.9.2 (E)-3-(3,4-dimethoxyphenyl)-1-(2,6-dimethoxypyridin-4-yl)prop-2-en-1-one (**15b**). Yellow solid, yield 72.3%. ^{1}H NMR (300 MHz, $CDCl_3$) δ 7.59 (d, *J* = 15.7 Hz, 1H), 7.09 – 6.98 (m, 3H), 6.75 (d, *J* = 8.3 Hz, 1H), 6.63 (s, 2H), 3.83 (s, 6H), 3.81 (s, 3H), 3.79 (s, 3H), ^{13}C NMR (75 MHz, $CDCl_3$) δ 189.87, 163.85, 151.84, 150.69, 149.31, 146.50, 127.43, 123.71, 119.76, 111.11, 109.96, 99.86, 56.00, 55.96, 53.89. HR-MS (ESI) *m/z*: calcd for $C_{18}H_{20}NO_5$ $[M+H]^+$ 330.1336, found 330.1331.

4.1.9.3 (E)-1-(2,6-dimethoxypyridin-4-yl)-3-(3,4,5-trimethoxyphenyl)prop-2-en-1-one (**15c**). Yellow solid, yield 83.7%. ^{1}H NMR (300 MHz, $CDCl_3$) δ 7.57 (d, *J* = 15.7 Hz, 1H), 7.10 (s, 1H), 6.72 (s, 2H), 6.65 (s, 2H), 3.86 (s, 6H), 3.80 (s, 6H), 3.78 (s, 3H), ^{13}C NMR (75 MHz, $CDCl_3$) δ 189.88, 163.89, 153.51, 150.47, 146.49, 140.88, 129.87, 121.20, 105.88, 99.92, 61.01, 56.25, 53.92; HR-MS (ESI) *m/z*: calcd for $C_{19}H_{22}NO_6$ $[M+H]^+$ 360.1442, found 360.1440.

4.1.9.4 (E)-1-(2,6-dimethoxypyridin-4-yl)-3-(4-(methylthio)phenyl)prop-2-en-1-one (**15d**). Yellow solid, yield 77.6%. ^{1}H NMR (300 MHz, $CDCl_3$) δ 7.74 (d, *J* = 15.7 Hz, 1H), 7.53 (d, *J* = 8.1 Hz, 2H), 7.30 (s, 1H), 7.24 (d, *J* = 5.0 Hz, 2H), 6.77 (s, 2H), 3.97 (s, 6H), 2.52 (s, 3H); ^{13}C NMR (75 MHz, $CDCl_3$) δ 205.60, 163.92, 156.40, 150.51, 145.81, 128.97, 125.92, 120.80, 99.86, 98.74, 53.93, 15.06. HR-MS (ESI) *m/z*: calcd for $C_{17}H_{18}NO_3S$ $[M+H]^+$ 316.1002, found 316.0998.

4.1.9.5

(E)-1-(2,6-dimethoxypyridin-4-yl)-3-(3-hydroxy-4-methoxyphenyl)prop-2-en-1-one

(**15e**). Yellow solid, yield 57.3%. ^{1}H NMR (300 MHz, $CDCl_3$) δ 7.71 (d, *J* = 15.7 Hz, 1H), 7.25 (d, *J* = 3.0 Hz, 1H), 7.21 (s, 1H), 7.15– 7.11 (m, 1H), 6.88 (d,*J* = 8.3 Hz, 1H), 6.76 (s, 2H), 5.68 (s, 1H), 3.97 (s, 6H), 3.95 (s, 3H), ^{13}C NMR (75 MHz, $CDCl_3$) δ 163.60, 163.36, 161.07, 153.08, 152.69, 149.77, 136.54, 106.04, 105.03, 99.33, 98.74, 98.03, 56.15, 53.65. HR-MS (ESI) *m/z*: calcd for $C_{17}H_{18}NO_5$ $[M+H]^+$316.1179, found 316.1174.

4.1.9.6

(E)-1-(2,6-dimethoxypyridin-4-yl)-3-(3-fluoro-4-methoxyphenyl)prop-2-en-1-one

(**15f**). White solid, yield 63.7%. ^{1}H NMR (300 MHz, $CDCl_3$) δ 7.56 (d, *J* = 15.7 Hz, 1H), 7.24 (t, *J* = 11.2 Hz, 2H), 7.05 (d, *J* = 15.7 Hz, 1H), 6.85 (t, *J* = 8.4 Hz, 1H), 6.63 (s, 2H), 3.85 (s, 6H), 3.81 (s, 3H), ^{13}C NMR (75 MHz, $CDCl_3$) δ 189.61, 163.93, 154.05, 150.36, 150.04 (d,*J* = 24.0 Hz), 147.85, 146.01, 144.95, 127.69, 126.31, 123.80, 120.75 (d,*J* = 228.8 Hz), 115.15, 114.90 (d, *J* = 18.8 Hz), 113.21, 99.83, 56.27, 53.91; HR-MS (ESI)*m/z*: calcd for $C_{17}H_{17}FNO_4$ $[M+H]^+$ 318.1136, found 318.1140.

4.1.9.7

(E)-1-(2,6-dimethoxypyridin-4-yl)-3-(4-methoxyphenyl)-2-methylprop-2-en-1-one

(**16a**). Yellow solid, yield 78.7%. ^{1}H NMR (300 MHz, $CDCl_3$) δ 7.40 (d, *J* = 8.4 Hz, 2H), 7.23 (s, 1H), 6.96 – 6.89 (m, 2H), 6.46 (s, 2H), 3.96 (s, 6H), 3.85 (s, 3H), 2.23 (s, 3H), ^{13}C NMR (75 MHz, $CDCl_3$) δ 197.33, 162.70, 159.85, 151.75, 144.55, 133.53, 131.43, 127.49, 113.52, 100.07, 54.86, 53.29, 12.99. HR-MS (ESI) *m/z*: calcd for $C_{20}H_{24}NO_6$ $[M+H]^+$ 374.1598, found 313.1596.

4.1.9.8

(E)-3-(3,4-dimethoxyphenyl)-1-(2,6-dimethoxypyridin-4-yl)-2-methylprop-2-en-1-one

(**16b**). Yellow solid, yield 86.9%. ^{1}H NMR (300 MHz, $CDCl_3$) δ 7.22 (s, 1H), 7.07 (d, *J* = 8.0 Hz, 1H), 6.95 – 6.89 (m, 2H), 6.46 (s, 2H), 3.96 (s, 6H), 3.93 (s, 3H), 3.90 (s, 3H), 2.26 (s, 3H), ^{13}C NMR (75 MHz, $CDCl_3$) δ 197.26, 162.72, 151.73, 149.49, 148.25, 144.67, 133.82, 127.73, 123.30, 112.58, 110.41, 100.07, 55.46, 53.30, 13.07. HR-MS (ESI) *m/z*: calcd for $C_{19}H_{22}NO_5$ $[M+H]^+$ 344.1492, found 313.1493.

4.1.9.9

(E)-1-(2,6-dimethoxypyridin-4-yl)-2-methyl-3-(3,4,5-trimethoxyphenyl)prop-2-en-1-one (**16c**). Yellow solid, yield 85.3%. ^{1}H NMR (300 MHz, $CDCl_3$) δ 7.19 (s, 1H), 6.64 (s, 2H), 6.47 (s, 2H), 3.97 (s, 6H), 3.89 (s, 3H), 3.88 (s, 6H), 2.25 (s, 3H), ^{13}C NMR (75 MHz, $CDCl_3$) δ 197.17, 162.76, 152.59, 151.40, 144.43, 138.52, 134.97, 130.29, 106.93, 100.10, 60.47, 55.74, 53.31, 13.16. HR-MS (ESI) *m/z*: calcd for $C_{18}H_{20}NO_4$ $[M+H]^+$ 313.1387, found 313.1385.

4.1.9.10

(E)-1-(2,6-dichloropyridin-4-yl)-3-(3-hydroxy-4-methoxyphenyl)-2-methylprop-2-en-1-one (**16d**). Yellow solid, yield 75.1%. ^{1}H NMR (300 MHz, $CDCl_3$) δ 7.13 (s, 1H), 7.09 (s, 1H), 7.04 (s, 1H), 6.96 (d, *J* = 9.5 Hz, 1H), 6.89 (d, *J* = 8.8 Hz, 1H), 6.77 (s, 1H), 3.95 (s, 3H), 2.24 (s, 3H), ^{13}C NMR (75 MHz, $CDCl_3$) δ 198.78, 160.43, 141.55, 135.76, 131.55, 126.42, 123.28, 120.95, 118.52, 111.52, 107.06, 103.53, 55.57, 15.01. HR-MS (ESI) *m/z*: calcd for $C_{16}H_{14}Cl_2NO_3$ $[M+H]^+$ 338.0345, found 338.0352.

4.1.9.11

(E)-1-(2-chloro-6-methoxypyridin-4-yl)-3-(3-hydroxy-4-methoxyphenyl)-2-methylprop-2-en-1-one (**16e**). Yellow solid, yield 65.2%. ^{1}H NMR (300 MHz, DMSO-d_6) δ 9.24 (s, 1H), 7.19 (s, 1H), 7.11 (s, 1H), 7.06 (s, 1H), 7.00 (s, 2H), 6.93 (s, 1H), 3.91 (s, 3H), 3.82 (s, 3H), 2.15 (s, 3H), ^{13}C NMR (75 MHz, $CDCl_3$) δ 197.26, 162.70, 147.23, 144.57, 136.24, 133.68, 128.15, 127.51, 126.98, 126.69, 124.14, 115.28, 110.85, 100.06, 55.51, 53.30, 12.86. HR-MS (ESI) *m/z*: calcd for $C_{17}H_{17}ClNO_4$ $[M+H]^+$ 334.0841, found 334.0834.

4.1.9.12

(E)-1-(2,6-dimethoxypyridin-4-yl)-3-(3-hydroxy-4-methoxyphenyl)-2-methylprop-2-en-1-one (**16f**). Yellow solid, yield 75.3%. ^{1}H NMR (300 MHz, $CDCl_3$) δ 7.18 (s, 1H), 7.08 (d, *J* = 2.1 Hz, 1H), 6.97 – 6.92 (m, 1H), 6.87 (d, *J* = 8.5 Hz, 1H), 6.45 (s, 2H), 5.64 (s, 1H), 3.96 (s, 6H), 3.94 (s, 3H), 2.23 (s, 3H), ^{13}C NMR (75 MHz, $CDCl_3$) δ 162.72, 151.65, 146.91, 144.95, 144.51, 128.36, 127.81, 127.44, 122.83, 115.47, 109.87, 100.10, 55.49, 53.30, 13.01. HR-MS (ESI) *m/z*: calcd for $C_{18}H_{20}NO_5$ $[M+H]^+$ 330.1336, found 330.1332.

*4.1.10 The procedure for the preparation of **18a-i**.*

To a stirred solution of ketone **9b** (50 mg, 0.34 mmol) and aldehyde (0.34 mmol) in anhydrous EtOH, piperidine (144.9 mg, 1.72 mmol) was slowly added. After stirring for 10 h at 80 °C, the reaction mixture was concentrated and extracted with CH_2Cl_2 (3 × 20 mL). The combined organic layers were then washed with brine, dried over anhydrous Na_2SO_4, and concentrated in vacuo to provide the crude product, which was purified by column chromatography with petroleum/ethyl acetate (4:1) to give the corresponding pure compounds ***18a-i***.

4.1.10.1

(E)-1-(2,6-dimethoxypyridin-4-yl)-3-(1H-indol-3-yl)-2-methylprop-2-en-1-one (**18a**). Yellow solid, yield 85.9%. ^{1}H NMR (300 MHz, $CDCl_3$) δ 8.74 (s, 1H), 7.70 (s, 1H), 7.65 (d, *J* = 2.9 Hz, 1H), 7.54 (d, *J* = 7.8 Hz, 1H), 7.43 (d, *J* = 8.0 Hz, 1H), 7.29 (d, *J* = 7.5 Hz, 1H), 7.19 (d, *J* = 7.3 Hz, 1H), 6.51 (s, 2H), 3.98 (s, 6H), 2.28 (s, 3H), ^{13}C NMR (75 MHz, DMSO-d_6) δ 195.46, 162.62, 153.39, 137.13, 135.76, 129.10, 128.89, 127.15, 122.59, 120.57, 117.59, 112.13, 111.21, 99.95, 53.52, 13.77. HR-MS (ESI) *m/z*: calcd for $C_{19}H_{19}N_2O_3[M+H]^+$ 323.1390, found 323.1388.

4.1.10.2

(E)-1-(2,6-dimethoxypyridin-4-yl)-3-(5-methoxy-1H-indol-3-yl)-2-methylprop-2-en-1-one (**18b**). Yellow solid, yield 77.9%. ^{1}H NMR (300 MHz, $CDCl_3$) δ 8.66 (s, 1H), 7.63 (d, *J* = 10.0 Hz, 2H), 7.32 (d, *J* = 8.7 Hz, 1H), 6.93 (d, *J* = 10.9 Hz, 2H), 6.52 (s, 2H), 3.97 (s, 6H), 3.84 (s, 3H), 2.26 (s, 3H), ^{13}C NMR (75 MHz, $CDCl_3$) δ 196.85, 163.22, 155.22, 136.87, 131.52, 130.81, 130.53, 128.26, 127.16, 113.21, 112.15, 110.40, 101.08, 100.70, 55.92, 53.78, 14.29. HR-MS (ESI) *m/z*: calcd for $C_{20}H_{21}N_2O_4[M+H]^+$ 353.1496, found 353.1497.

4.1.10.3

(E)-1-(2,6-dimethoxypyridin-4-yl)-3-(6-methoxy-1H-indol-3-yl)-2-methylprop-2-en-1-one (**18c**). Yellow solid, yield 78.3%. ^{1}H NMR (300 MHz, $CDCl_3$) δ 8.62 (s, 1H), 7.64 (s, 1H), 7.53 (d, *J* = 2.8 Hz, 1H), 7.40 (d, *J* = 8.6 Hz, 1H), 6.89 (d, *J* = 2.1 Hz, 1H), 6.85 (dd, *J* = 8.7, 2.2 Hz, 1H), 6.49 (s, 2H), 3.97 (s, 6H), 3.85 (s, 3H), 2.25 (s, 3H), ^{13}C NMR (75 MHz, $CDCl_3$) δ 196.50, 162.71, 156.89, 152.44, 148.19, 136.68, 130.68, 125.14, 121.14, 118.81, 112.85, 110.56, 100.05, 94.23, 55.18, 53.32, 13.67.

HR-MS (ESI) *m/z*: calcd for $C_{20}H_{21}N_2O_4[M+H]^+$ 353.1496, found 353.1499.

4.1.10.4

(E)-1-(2,6-dimethoxypyridin-4-yl)-3-(5-fluoro-1H-indol-3-yl)-2-methylprop-2-en-1-on e (**18d**). Yellow solid, yield 66.5%. ^{1}H NMR (300 MHz, $CDCl_3$) δ 8.76 (s, 1H), 7.68 (s, 1H), 7.56 (s, 1H), 7.35 (d, *J* = 8.2 Hz, 1H), 7.17 (d, *J* = 9.2 Hz, 1H), 7.04 (d, *J* = 9.2 Hz, 1H), 6.49 (s, 2H), 3.99 (s, 6H), 2.26 (s, 3H), ^{13}C NMR (75 MHz, DMSO-d_6) δ 196.03, 163.11, 153.58, 137.14, 132.90, 131.22, 129.64, 113.88 (d, *J* = 186.8 Hz), 113.75, 111.94, 111.39, 111.03, 103.63, 103.31, 100.58, 53.97, 14.40. HR-MS (ESI) *m/z*: calcd for $C_{19}H_{18}FN_2O_3[M+H]^+$ 341.1296, found 341.1298.

4.1.10.5

(E)-1-(2,6-dimethoxypyridin-4-yl)-3-(6-fluoro-1H-indol-3-yl)-2-methylprop-2-en-1-on e (**18e**). Yellow solid, yield 66.5%. ^{1}H NMR (300 MHz, $CDCl_3$) δ 8.73 (s, 1H), 7.62 (s, 2H), 7.47 – 7.41 (m, 1H), 7.11 (d, *J* = 8.9 Hz, 1H), 7.00– 6.92 (m, 1H), 6.50 (s, 2H), 3.98 (s, 6H), 2.26 (s, 3H), ^{13}C NMR (75 MHz, $CDCl_3$) δ 197.00, 163.24, 152.69, 136.41, 131.81, 126.82, 124.02, 119.67, 119.54, 113.30, 110.08 (d, *J* = 241.5 Hz), 109.76, 100.56, 98.05, 97.70, 53.84, 14.23. HR-MS (ESI) *m/z*: calcd for $C_{19}H_{18}FN_2O_3[M+H]^+$ 341.1296, found 341.1296.

4.1.10.6

(E)-3-(5-chloro-1H-indol-3-yl)-1-(2,6-dimethoxypyridin-4-yl)-2-methylprop-2-en-1-o ne (**18f**). Yellow solid, yield 73.5%. ^{1}H NMR (300 MHz, $CDCl_3$) δ 8.68 (s, 1H), 7.66 (s, 1H), 7.55 (s, 1H), 7.49 (s, 1H), 7.35 (d, *J* = 8.8 Hz, 2H), 6.49 (s, 2H), 3.99 (s, 6H), 2.26 (s, 3H), ^{13}C NMR (75 MHz, DMSO-d_6) δ 196.10, 163.10, 153.50, 136.78, 134.79, 130.95, 130.13, 128.83, 125.63, 123.06, 117.75, 114.21, 111.51, 100.64, 54.00, 14.48. HR-MS (ESI) *m/z*: calcd for $C_{19}H_{18}ClN_2O_3[M+H]^+$ 357.1000, found 357.1001. *4.1.10.7*

(E)-3-(6-chloro-1H-indol-3-yl)-1-(2,6-dimethoxypyridin-4-yl)-2-methylprop-2-en-1-o ne (**18g**). Yellow solid, yield 53.7%. ^{1}H NMR (300 MHz, $CDCl_3$) δ 8.75 (s, 1H), 7.64 – 7.58 (m, 2H), 7.42 (s, 1H), 7.16 (dd, *J* = 8.4, 1.9 Hz, 1H), 6.74 (s, 1H), 6.50 (s, 2H), 3.98 (s, 6H), 2.26 (s, 3H), ^{13}C NMR (75 MHz, $CDCl_3$) δ 200.37, 163.25, 152.62, 136.18, 135.85, 131.91, 129.38, 127.01, 126.00, 121.85, 119.63, 113.33, 111.43,

100.56, 53.84, 14.27. HR-MS (ESI) *m/z*: calcd for $C_{19}H_{18}ClN_2O_3[M+H]^+$ 357.1000, found 357.1002.

4.1.10.8

(E)-1-(2,6-dimethoxypyridin-4-yl)-3-(1H-indol-5-yl)-2-methylprop-2-en-1-one (**18h**). Yellow solid, yield 86.1%. ^{1}H NMR (300 MHz, $CDCl_3$) δ 8.37 (s, 1H), 7.73 (s, 1H), 7.43 (d, *J* = 6.5 Hz, 1H), 7.27 (d, *J* = 4.7 Hz, 3H), 6.57 (s, 2H), 6.43 (s, 1H), 3.97 (s, 6H), 2.25 (s, 3H), ^{13}C NMR (75 MHz, $CDCl_3$) δ 197.54, 162.79, 151.63, 142.75, 135.59, 135.24, 127.13, 126.95, 124.45, 121.29, 120.41, 111.64, 100.77, 100.25, 53.34, 13.52. HR-MS (ESI) *m/z*: calcd for $C_{19}H_{19}N_2O_3[M+H]^+$ 323.1390, found 323.1395.

4.1.10.9

(E)-1-(2,6-dimethoxypyridin-4-yl)-3-(1H-indol-6-yl)-2-methylprop-2-en-1-one (**18i**). Yellow solid, yield 56.3%. ^{1}H NMR (300 MHz, $CDCl_3$) δ 8.48 (s, 1H), 7.77 (s, 1H), 7.46 (s, 1H), 7.39 (d, *J* = 8.5 Hz, 1H), 7.29 (d, *J* = 1.7 Hz, 1H), 7.23 (s, 1H), 6.58 (s, 1H), 6.50 (s, 2H), 3.96 (s, 6H), 2.32 (s, 3H), ^{13}C NMR (75 MHz, $CDCl_3$) δ 198.18, 163.23, 152.64, 147.59, 136.14, 133.51, 128.02, 127.27, 125.37, 124.62, 123.51, 111.15, 103.38, 100.61, 53.78, 13.59. HR-MS (ESI) *m/z*: calcd for $C_{19}H_{19}N_2O_3[M+H]^+$ 323.1390, found 323.1393.

4.1.11

(E)-1-(2,6-dimethoxypyridin-4-yl)-2-methyl-3-(1-methyl-1H-indol-3-yl)prop-2-en-1-one (**19a**). To a solution of **18a** (90 mg, 0.28 mmol) in anhydrous DMF was added NaH (10 mg, 0.42 mmol), MeI (52 mg, 0.36 mmol). After stirring at room temperature for 2 h, the mixture was diluted with water and extracted with ethyl acetate (3 × 20 mL). The combined organic layers were then washed with brine, dried over anhydrous Na_2SO_4, and concentrated in vacuo to provide the crude product, which was purified by column chromatography with petroleum/ethyl acetate (4:1) to give the **19a** as yellow solid (70 mg, 78.02 %). ^{1}H NMR (300 MHz, $CDCl_3$) δ 7.69 (s, 1H), 7.52 (s, 2H), 7.34 (d, *J* = 12.3 Hz, 2H), 7.22 (d, *J* = 7.4 Hz, 1H), 6.53 – 6.45 (m, 2H), 3.98 (s, 6H), 3.90 (s, 3H), 2.27 (s, 3H), ^{13}C NMR (75 MHz, $CDCl_3$) δ 196.82, 163.19, 153.14, 137.08, 136.60, 131.33, 130.09, 128.26, 123.15, 120.97, 118.66,

111.90, 109.72, 100.56, 53.82, 33.50, 14.24. HR-MS (ESI) *m/z*: calcd for $C_{20}H_{21}N_2O_3[M+H]^+$ 337.1547, found 337.1544.

4.1.12

(E)-1-(2,6-dimethoxypyridin-4-yl)-3-(1-ethyl-1H-indol-3-yl)-2-methylprop-2-en-1-one (**19b**). To a solution of **18a** (90 mg, 0.28 mmol) in anhydrous DMF was added NaH (10 mg, 0.42 mmol), iodoethane (56.6 mg, 0.36 mmol). After stirring at room temperature for 2 h, the mixture was diluted with water and extracted with ethyl acetate (3 × 20 mL). The combined organic layers were then washed with brine, dried over anhydrous Na_2SO_4, and concentrated in vacuo to provide the crude product, which was purified by column chromatography with petroleum/ethyl acetate (4:1) to give the **19b** as yellow solid (60 mg, 72.3.2 %). ^{1}H NMR (300 MHz, $CDCl_3$) δ 7.70 (s, 1H), 7.57 (s, 1H), 7.53 (d, *J* = 8.0 Hz, 1H), 7.37 (s, 1H), 7.31 (d, *J* = 7.3 Hz, 1H), 7.18 (d, *J* = 7.4 Hz, 1H), 6.49 (s, 2H), 4.27 (d, *J* = 7.3 Hz, 2H), 3.97 (s, 6H), 2.27 (s, 3H), 1.54 (s, 3H), ^{13}C NMR (75 MHz, $CDCl_3$) δ 196.85, 163.19, 153.17, 137.19, 135.63, 130.03, 129.67, 128.47, 123.04, 120.93, 118.80, 112.02, 109.81, 100.55, 53.82, 41.77, 15.34, 14.26. HR-MS (ESI) *m/z*: calcd for $C_{21}H_{23}N_2O_3[M+H]^+$ 351.1703, found 351.1699.

4.1.13

(E)-1-(2,6-dimethoxypyridin-4-yl)-3-(1-(hydroxymethyl)-1H-indol-3-yl)-2-methylprop-2-en-1-one (**19c**). To a solution of **18a** (100 mg, 0.31 mmol) in anhydrous EtOH was added HCHO (37% in water, 1 mL), NaOH (6 N, 2 mL). After stirring at 80 °C for 2 h, the reaction mixture was concentrated and extracted with CH_2Cl_2 (3 × 20 mL). The combined organic layers were then washed with brine, dried over anhydrous Na_2SO_4, and concentrated in vacuo to provide the crude product, which was purified by column chromatography with petroleum/ethyl acetate (4:1) to give the **19c** as yellow solid (60 mg, 55.04 %). ^{1}H NMR (300 MHz, $CDCl_3$) δ 7.62 (d, *J* = 4.6 Hz, 2H), 7.50 (d, *J* = 8.0 Hz, 2H), 7.31 - 7.18 (m, 2H), 6.43 (s, 2H), 5.69 (s, 2H), 3.95 (s, 6H), 2.21 (s, 3H), ^{13}C NMR (75 MHz, $CDCl_3$) δ 197.24, 163.20, 152.62, 136.95, 135.47, 131.20, 129.64, 128.77, 123.64, 121.61, 118.85, 113.06, 110.12, 100.53, 70.40, 53.83, 14.28. HR-MS (ESI) *m/z*: calcd for $C_{20}H_{21}N_2O_4[M+H]^+$ 353.1496, found 353.1492.

4.1.14

(E)-3-(1-acetyl-1H-indol-3-yl)-1-(2,6-dimethoxypyridin-4-yl)-2-methylprop-2-en-1-one (**19d**).

To a solution of **18a** (100 mg, 0.31 mmol) in anhydrous DCM was added NaOH (31 mg, 0.78 mmol), acetylchloride (36.5 mg, 0.47 mmol). After stirring at room temperature for 2 h, the mixture was quenched with water and extracted with ethyl acetate (3 × 20 mL). The combined organic layers were then washed with brine, dried over anhydrous Na_2SO_4, and concentrated in vacuo to provide the crude product, which was purified by column chromatography with petroleum/ethyl acetate (4:1) to give the **19d** as yellow solid (80 mg, 70.80 %). ^{1}H NMR (300 MHz, $CDCl_3$) δ 8.43 (d, *J* = 8.2 Hz, 1H), 7.73 (s, 1H), 7.50 – 7.39 (m, 3H), 7.34 (d, *J* = 7.6 Hz, 1H), 6.52 (s, 2H), 3.98 (s, 6H), 2.74 (s, 3H), 2.31 (s, 3H), ^{13}C NMR (75 MHz, $CDCl_3$) δ 196.80, 168.48, 163.34, 151.68, 135.82, 133.87, 129.72, 126.22, 125.72, 124.21, 118.72, 117.84, 116.61, 100.64, 53.86, 24.14, 14.74. HR-MS (ESI) *m/z*: calcd for $C_{21}H_{21}N_2O_4[M+H]^+$ 365.1496, found 365.1495.

4.1.15

(E)-1-(2,6-dimethoxypyridin-4-yl)-3-(1-(furan-2-carbonyl)-1H-indol-3-yl)-2-methylprop-2-en-1-one (**19e**).

To a solution of **18a** (100 mg, 0.31 mmol) in anhydrous DCM was added NaOH (31 mg, 0.78 mmol), 2-furoyl chloride (61.3 mg, 0.47 mmol). After stirring at room temperature for 2 h, the mixture was quenched with water and extracted with ethyl acetate (3 × 20 mL). The combined organic layers were then washed with brine, dried over anhydrous Na_2SO_4, and concentrated in vacuo to provide the crude product, which was purified by column chromatography with petroleum/ethyl acetate (4:1) to give the **19e** as yellow solid (92 mg, 71.32 %). ^{1}H NMR (300 MHz, $CDCl_3$) δ 8.47 (d, *J* = 8.2 Hz, 1H), 8.39 (s, 1H), 7.77 (s, 1H), 7.52 (d, *J* = 5.1 Hz, 2H), 7.42 (d, *J* = 7.8 Hz, 1H), 7.36 (d, *J* = 7.4 Hz, 1H), 7.26 (s, 1H), 6.70 (s, 1H), 6.53 (s, 2H), 3.99 (s, 6H), 2.32 (s, 3H), ^{13}C NMR (75 MHz, $CDCl_3$) δ 211.32, 196.82, 163.35, 153.37, 151.78, 146.78, 136.09, 135.71, 134.11, 129.54, 127.20, 125.99, 124.54, 121.43, 118.66, 117.97, 116.68, 112.74, 100.66, 53.85, 14.62. HR-MS (ESI) *m/z*: calcd for

$C_{24}H_{21}N_2O_5[M+H]^+$ 417.1445, found 417.1447.

4.1.16

(E)-3-(1-benzoyl-1H-indol-3-yl)-1-(2,6-dimethoxypyridin-4-yl)-2-methylprop-2-en-1-one (**19f**).

To a solution of **18a** (100 mg, 0.31 mmol) in anhydrous DCM was added NaOH (31 mg, 0.78 mmol), benzoyl chloride (66.1 mg, 0.47 mmol). After stirring at room temperature for 2 h, the mixture was quenched with water and extracted with ethyl acetate (3 × 20 mL). The combined organic layers were then washed with brine, dried over anhydrous Na_2SO_4, and concentrated in vacuo to provide the crude product, which was purified by column chromatography with petroleum/ethyl acetate (4:1) to give the **19f** as yellow solid (100 mg, 75.76 %).^{1}H NMR (300 MHz, $CDCl_3$) δ 8.34 (d, *J* = 8.2 Hz, 1H), 7.83 - 7.77 (m, 2H), 7.62 (dq, *J* = 14.8, 7.4 Hz, 4H), 7.52 – 7.36 (m, 4H), 6.50 (s, 2H), 3.98 (s, 6H), 2.16 (s, 3H), ^{13}C NMR (75 MHz, $CDCl_3$) δ 196.76, 168.49, 163.33, 151.73, 135.75, 133.94, 133.86, 132.62, 129.98, 129.32, 128.86, 128.17, 125.95, 124.43, 118.80, 117.24, 116.39, 100.63, 53.85, 14.54. HR-MS (ESI) *m/z*: calcd for $C_{26}H_{23}N_2O_4[M+H]^+$ 427.1652, found 427.1653.

4.1.17

(E)-1-(2,6-dimethoxypyridin-4-yl)-2-methyl-3-(1-methyl-1H-indol-5-yl)prop-2-en-1-one (**19g**).

To a solution of **18h** (90 mg, 0.28 mmol) in anhydrous DMF was added NaH (10 mg, 0.42 mmol), MeI (52 mg, 0.36 mmol). After stirring at room temperature for 2 h, the mixture was diluted with water and extracted with ethyl acetate (3 × 20 mL). The combined organic layers were then washed with brine, dried over anhydrous Na_2SO_4, and concentrated in vacuo to provide the crude product, which was purified by column chromatography with petroleum/ethyl acetate (4:1) to give the **19g** as yellow solid (75 mg, 83.59 %).^{1}H NMR (300 MHz, $CDCl_3$) δ 7.77 (s, 1H), 7.46 (s, 1H), 7.33 (s, 2H), 7.10 (d, *J* = 3.1 Hz, 1H), 6.53 (d, *J* = 3.2 Hz, 1H), 6.49 (s, 2H), 3.96 (s, 6H), 3.82 (s, 3H), 2.32 (s, 3H), ^{13}C NMR (75 MHz, $CDCl_3$) δ 192.51, 163.19, 137.20, 130.75, 129.70, 128.53, 126.42, 123.03, 121.78, 120.93, 118.78, 109.82, 103.22, 100.55, 53.82, 41.76, 14.26. HR-MS (ESI) *m/z*: calcd for $C_{20}H_{21}N_2O_3[M+H]^+$

337.1547, found 337.1544.

4.2 Pharmacology

4.2.1 In vitro antiproliferative assay

Cells were purchased from Nanjing KeyGen Biotech Co. Ltd. (Nanjing, China). The cytotoxicity of the test compounds was determined using the MTT assay. Briefly, the cell lines were incubated at 37 °C in a humidified 5% CO_2 incubator for 24 h in 96-microwell plates. After medium removal, 100 mL of culture medium with 0.1% DMSO containing the test compounds at different concentrations was added to each well and incubated at 37 °C for another 72 h. The MTT (5 mg/mL in PBS) was added and incubated for another 4 h, the optical density was detected with a microplate reader at 490 nm. The IC_{50} values were calculated according to the dose-dependent curves. All the experiments were repeated in at least three independent experiments.

4.2.2 In vitro tubulin polymerization inhibitory assay

An amount of 2 mg/mL tubulin (Cytoskeleton) was resuspended in PEM buffer containing 80 mM piperazine-N,N'-bis(2-ethanesulfonic acid) sequisodium salt PIPES (pH 6.9), 0.5 mM EGTA, 2 mM $MgCl_2$, and 15% glycerol. Then the mixture was preincubated with tested compounds or vehicle DMSO on ice. PEG containing GTP was added to the final concentration of 3 mg/mL before detecting the tubulin polymerization reaction. After 30 min, the absorbance was detected by a spectrophotometer at 340 nm at 37 °C every 2 min for 60 min. The area under the curve was used to determine the concentration that inhibited tubulin polymerization by 50% (IC_{50}), which was calculated with GraphPad Prism Software version 5.02.

4.2.3 Competitive Inhibition Assays.

The competitive binding activity of tested compounds was evaluated using a radiolabeled [3H]colchicine competition scintillation proximity (SPA) assay. In brief, 0.08 μM [3H]colchicine was mixed with **16f** (1 μM, 5 μM) or CA-4 (1 μM, 5 μM) and biotinylated porcine tubulin (0.5 μg) in a buffer of 100 μL containing 80 mM PIPES (pH 6.8), 1 mM EGTA, 10% glycerol, 1 mM $MgCl_2$, and 1 mM GTP for 2 h at 37 °C.

Then streptavidin-labeled SPA beads (80 μg) were added to each mixture. The radioactive counts were measured directly with a scintillation counter.

4.2.4 Immunofluorescence Staining

K562 cells or MDA-MB-231 cells were seeded into 6-well plates and then treated with vehicle control 0.1% DMSO, **16f** (10, 20, 40 nM) or **16f** (20, 40, 80 nM) respectively. The cells were fixed with 4% paraformaldehyde and then penetrated with PBS for three times. After blocking for 20 min by adding 50-100 μL goat serum albumin at room temperature, cells were incubated with a monoclonal antibody (anti-α-tubulin) at 37 °C for 2 h. Then the cells were washed three times by PBS following staining by fluorescence antibody and labeling of nuclei by 4,6-diamidino-2-phenylindole (DAPI). Cells were finally visualized using an LSM 570 laser confocal microscope (Carl Zeiss, Germany).

4.2.5 Cell cycle analysis

K562 cells were seeded into 6-well plates and incubated at 37 °C in a humidified 5% CO_2 incubator for 24 h, and then treated with or without **16f** at indicated concentrations for another 48 h. The collected cells were fixed by adding 70% ethanol at 4 °C for 12 h. Subsequently, the cells were resuspended in PBS containing 100 mL RNase A and 400 mL of propidium iodide for 30 min. The DNA content of the cells was measured using a FACS Calibur flow cytometer (Bectone Dickinson, San Jose, CA, USA).

4.2.6 Cell apoptosis analysis

After treatment with or without **16f** at indicated concentrations for 48 h, the cells were washed twice in PBS, centrifuged and resuspended in 500 mL AnnexinV binding buffer. The cells were then harvested, washed and stained with 5 mL Annexin V-APC and 5 mL 7-AAD in the darkness for 15 min. Apoptosis was analyzed using a FACS Calibur flow cytometer (Bectone Dickinson, San Jose, CA, USA).

4.2.7 Mitochondrial Membrane Potential Analysis

After treatment with vehicle control 0.1% DMSO, **16f** (10 nM, 20 nM, and 40 nM) for 24 h, the cells were washed in PBS and resuspended in 500 mL JC-1 incubation buffer at 37 °C for 15 min. The percentage of cells with healthy or collapsed mitochondrial membrane potentials was monitored by flow cytometry analysis (Bectone-Dickinson, San Jose, CA, USA).

4.2.8 Wound healing assay

K562 cells were grown in 6-well plates for 24 h. Scratches were made in confluent monolayers using 200 μL pipette tip. Then, wounds were washed twice with PBS to remove non-adherent cell debris. The media containing different concentrations (1, 2, 4 nM) of the compound **16f** were added to the petridishes. Cells which migrated across the wound area were photographed using phase contrast microscopy at 0 h and 24 h. The migration distance of cells migrated in to the wound area was measured manually.

4.2.9 Tube formation assay

EC Matrigel matrix was thawed at 4 °C overnight, and HUVECs suspended in DMEM were seeded in 96-well culture plates at a cell density of 50,000 cells/well after polymerization of the Matrigel at 37 °C for 30 min. They were then treated with 20 μL different concentrations of compound **16f** or vehicle for 6 h at 37 °C. Then, the morphological changes of the cells and tubes formed were observed and photographed under inverted microscope (OLYMPUS, Japan).

4.2.10 In vivo antitumor evaluation

Five-week-old male Institute of Cancer Research (ICR) mice were purchased from Shanghai SLAC Laboratory Animals Co. Ltd. A total of 1×10^6 H22 cells were subcutaneously inoculated into the right flank of ICR mice according to protocols of tumor transplant research, to initiate tumor growth. After incubation for one day, mice were weighted and at random divided into eight groups of eight animals. The groups

treated with **16f** was administered 10, 20 mg/kg in a vehicle of 10% DMF/2% Tween 80/88% saline, respectively. The positive control group was treated with PTX (6 mg/kg) every 2 days by intravenous injection. CA-4 and CA-4P were administered 20 mg/kg in a vehicle of 10% DMF/2% Tween 80/88% saline and saline solution, respectively. The negative control group received a vehicle of 10% DMF/2% Tween 80/88% saline through intravenous injection. Treatments of **16f**, CA-4 and CA-4P were done at a frequency of intravenous injection one dose per day for a total 21 consecutive days while the positive group was treated with PTX one dose per two days. The mice were sacrificed after the treatments and the tumors were excised and weighed. The inhibition rate was calculated as follows: Tumor inhibitory ratio (%) = (1-average tumor weight of treated group/average tumor weight of control group) × 100%.

4.3 Molecular modeling

In our study, the X-ray structure of the DMDA-colchicine-*α*,*β*-tubulin complex was downloaded from the Protein Data Bank (PDB code 5lyj). The protein was prepared by removal of the stathmin-like domain, subunits C and D, water molecules and colchicine using Discovery Studio modules. The docking procedure was performed by employing DOCK program in Discovery Studio 3.0 software, and the structural image was obtained using PyMOL software.

Acknowledgments

This study was supported from the National Natural Science Foundation of China (nos. 81673306, 81703348), The Open Project of State Key Laboratory of Natural Medicines, China Pharmaceutical University (no. SKLNMKF 201710), China Postdoctoral Science Foundation (no. 2017100424) for financial support, and “Double First-Class” University project CPU2018GY04, China Pharmaceutical University

Reference

[1] J. Howard, A. Hyman, Dynamics and mechanics of the microtubule plus end, Nat. 422 (2003) 753-758.

[2] M. Jordan, L. Wilson, Microtubules as a target for anticancer drugs, Nat. Rev. Canc. 4 (2004) 253-265.

[3] C. Dumontet, M. Jordan, Microtubule-binding agents: a dynamic field of cancer therapeutics, Nat. Rev. Drug Discov. 9 (2010) 790-803.

[4] E. Porcù, R. Bortolozzi, G. Basso, G. Viola, Recent advances in vascular disrupting agents in cancer therapy, Future Med. Chem. 6 (2014) 1485-1498.

[5] S. Guggilapu, L. Guntuku, T. Reddy, A. Nagarsenkar, D. Sigalapalli, V.G.M. Naidu, S.K. Bhargava, N. Bathini, Synthesis of thiazole linked indolyl-3-glyoxylamide derivatives as tubulin polymerization inhibitors, Eur. J. Med. Chem. 138 (2017) 83-95.

[6] G. R. Pettit, S. B. Singh, M. R. Boyd, E. Hamel, R. K. Pettit, J. M. Schmidt, F. Hogan, Antineoplastic agents. 291. isolation and synthesis of combretastatins A-4, A-5, and A-6, J. Med. Chem. 38 (1995) 1666-1672.

[7] S. Ducki, R. Forrest, J. Hadfield, A. Kendall, N. Lawtence, A. McGowm, D. Rennison, Potent antimitotic and cell growth inhibitory properties of substituted chalcones, Bioorg. Med. Chem. Lett. 8 (1998) 1051-1056.

[8] R. Ravelli, B. Gigant, P. Curmi, I. Jourdan, S. Lachkar, A. SObel, M. Knossow, Insight into tubulin regulation from a complex with colchicine and a stathmin-like domain, Nature 428 (2004) 198-202.

[9] R. Gaspair, A. Prota, K. Bargsten, A. Cavalli, M. Steinmetz, Structural basis of *cis*- and *trans*-combretastain binding to tubulin, Chem. 2 (2017) 102-113.

[10] W. Li, H. Sun, S.Xu, Z. Zhu, J. Xu, Tubulin inhibitors targeting the colchicine binding site: a perspective of privileged structures, Future Med. Chem. 9 (2017) 1765-1794.

[11] Z. Wang, J. Chen, J. Wang, S. Ahn, C. Li, M., Y. Li, V. Loveless, J. Dalton, D. Miller, W. Li, Novel tubulin polymerization inhibitors overcome multidrug resistance and reduce melanoma lung metastasis, Pharm. Res. 29 (2012), 3040−3052.

[12] Q. Yue, X. Liu, D. Guo, Microtubule-binding natural products for cancer therapy,

Planta Med. 76 (2010) 1037−1043.

[13] X. Wu, Q. Wang, W. Li, Recent advances in heterocyclic tubulin inhibitors targeting the colchicine binding site, Anti-Cancer Agents Med. Chem. 16 (2016) 1325−1338.

[14] M. Dong, F. Liu, H. Zhou, S. Zhai, B. Yan, Novel natural product- and privileged scaffold-based tubulin inhibitors targeting the colchicine binding site, Molecules 21 (2016) 1375-1483.

[15] Y. Pang, B. An, L. Lou, J. Zhang, J. Yan, L. Huang, X. Li, S. Yin, Design, synthesis, and biological evaluation of novel selenium-containing isocombretastains and phenstatins as antitumor agents, J. Med. Chem. 60 (2017) 7300-7314.

[16] Q. Wang, K. Arnest, Y. Wang, G. Kumar, D. Ma, H. Chen, Z. Wu, J. Yang, S. White, D. Miller, W. Li, Structural modification of the 3,4,5-trimethoxyphenyl moiety in the tubulin inhibitor VERU-111 leads to improve antiproliferative activities, J. Med. Chem. 61 (2018) 7877-7891.

[17] M.A. Soussi, O. Provot, G. Bernadat, J. Bignon, D. Desravines, J. Dubois, J.D. Brion, S. Messaoudi, M. Alami, IsoCombretaQuinazolines: potent cytotoxic agents with antitubulin activity, Chem. Med. Chem. 10 (2015) 1392-1402.

[18] I. Khelifi, T. Naret, D. Renko, A. Hamze, G. Bernadat, J. Bignon, C. Lenoir, J. Dubois, J. Brion, O.Provot, M. Alami, Design, synthesis and anticancer properties of ioscombretaquinolines as potent tubulin assembly inhibitors, Eur. J. Med. Chem. 127 (2017) 1025-1034.

[19] S. Banerjee, K. Arnst, Y. Wang, G. Kumar, S. Deng, L. Yang, G. Li, J. Yang, S. White, W. Li, D. Miller, Heterocyclic-fused pyrimidines as novel tubulin polymerization inhibitors targeting the colchicine binding site: structural basis and antitumor efficacy, J. Med. Chem. 61 (2018) 1704-1718.

[20] W. Li, F. Xu, W. Shuai, H. Sun, H. Yao, S. Xu, H. Yao, Z. Zhu, D. Yang, Z. Chen, J. Xu, Discovery of novel quinoline-chalcone derivatives as potent anti-tumor agents with microtubule polymerization Inhibitory Activity, J. Med. Chem. 62 (2019) 993-1013.

[21] M. Wase, B. T. Worrell, J. Yu, Pd^0/PR3 - catalyzed arylation of nicotinic and isonicotinic acid derivatives, Angew. Chem. Int. Ed. 49 (2010) 1275-1277.

[22] I. Bonzheim, B. Mankel, P. Klapthor, J. Schmidt, T. Hinrichsen, O. Wachter, F. Fend, L.Quintanilla-Martinez, CALR-mutated essential thrombocythemia evolving to chronic myeloid leukemia with coexistent CALR mutation and BCR-ABL translocation, Blood 125 (2015) 2309-2311.

[23] C. J. Bailey, J. L. Gross, A. Pieters, A. Bastien, J. F. List, Effect of dapagliflozin in patients with type 2 diabetes who have inadequate glycaemic control with metformin: a randomised, double-blind, placebo-controlled trial, Lancet 375 (2010) 2223-2233.

[24] F. Liu, P. I. Boross, F. Wang, J. Tozser, J. M. Louis, R. W. Harrison, I. T. Weber, Kinetic, Stability, and structural changes in high-resolution crystal structures of HIV-1 protease with drug-resistant mutations L24I, I50V, and G73S, J. Mol. Biol. 354 (2005) 789-800.

[25] J. Wu, M. Zhang, D. Liu, Acalabrutinib (ACP-196): a selective second-generation BTK inhibitor, J. Hematol. Oncol. 9 (2016) 21-24.

[26] R. Kaur, G. Kaur, R. Gill, R. Soni, J. Bariwal, Recent developments in tubulin polymerization inhibitors: An overview, Eur. J. Med. Chem. 87 (2014) 89−124.

[27] W. Li, Y. Yin, H. Yao, W. Shuai, H. Sun, S. Xu, J. Liu, H. Yao, Z. Zhu, J. Xu, Discovery of novel vinyl sulfone derivatives as anti-tumor agents with microtubule polymerization inhibitory and vascular disrupting activities, Eur. J. Med. Chem. 157 (2018) 1068-1080.

[28] W. Li, W. Shuai, F. Xu, H. Sun, S. Xu, H. Yao, J. Liu, H. Yao, Z. Zhu, J. Xu, Discovery of novel 4- Arylisochromenes as anticancer agents inhibiting tubulin polymerization, ACS Med. Chem. Lett. 9 (2018) 974-979.

[29] W. Li, Y. Yin, W. Shuai, F. Xu, H. Yao, J. Liu, K. Cheng, J. Xu, Z. Zhu, S. Xu, Discovery of novel quinazolines as potential anti-tubulin agents occupying three zones of colchicine domain, Bioorg. Chem. 83 (2019) 380-390.

[30] W. Li, W. Shuai, H. Sun, F. Xu, Y. Bi, J. Xu, C. Ma, H. Yao, Z. Zhu, S. Xu, Design, synthesis and biological evaluation of quinoline-indole derivatives as

anti-tubulin agents targeting the colchicine binding site, Eur. J. Med. Chem. 163 (2019) 428-442.